orders actually belong to one disorder and are allelic, as suggested previously (Tomita et al. 1999).

We searched for mutations in almost all protein-coding genes mapped at the PKCCR. In addition, we also analyzed four ion-channel-related genes (*CACNG3*, *SCNN1B*, *SCNN1G*, and *CNGB1*), albeit located outside the PKCCR, since many episodic neurologic disorders, such as muscle diseases, epilepsy, and movement disorders, are known as ion-channel abnormalities (Bhatia et al. 2000). However, 14 coding exons in seven genes (Table 3) were not analyzed because of difficulties in PCR-amplification.

In the present study on a total of 157 genes, we failed to identify any causative mutations that can explain PKC in all of the seven families examined. However, two nonsynonymous substitutions, 6186C>A in exon 3 of *SCNN1G* and 45842A>G in exon 29 of *ITGAL*, which were co-segregated with PKC in Families C and F, respectively, which were not found in normal control individuals, might be implicated in PKC. In other words, they were not able to be totally ruled out from the candidacy for PKC. It thus remains to be investigated whether another mutation in either gene is found in other PKC families.

Although the mapping of PKC was successful in at least nine studies, causative mutations have been uncovered. This may imply that PKC is caused by aberrations other than exonic mutations, such as a deletion or insertion, in the promoter regions, including the 5′-UTR or 3′-UTR. However, there is still a possibility for usual exonic mutations in a novel gene not annotated in public databases. As PKC itself is, generally, a viable disorder with which patients may show high reproductive fitness, such a mutated allele may be transmitted through many generations. A chromosomal rearrangement is another possibility. The pericentromeric region of chromosome 16 has a large heterochromatin (C-band) block that contains several duplicated regions, through which, frequent chromosomal rearrangements occur (Loftus et al. 1999). It remains also to be seen whether PKC patients within a family share such a variant.

Acknowledgments We are indebted to the family members for their participation in this research. We especially thank Ms. Y. Noguchi and A. Goto for their technical assistance. N.N. was supported in part by a Grant-in-Aid for Scientific Research (Category S, grant no. 13854024; Priority Areas for Applied Genomics, grant no. 17019055) from the Ministry of Education, Culture, Sports, Science and Technology (MEXT) of Japan, and by Solution Oriented Research of Science and Technology (SORST) from the Japan Science and Technology Agency (JST). K.Y. was supported by a Grant-in-Aid for Scientific Research for Priority Areas (grant no. 17590288) from the MEXT of Japan.

References

Bennett LB, Roach ES, Bowcock AM (2000) A locus for paroxysmal kinesigenic dyskinesia maps to human chromosome 16. Neurology 54(1):125–130

Bhatia KP (1999) The paroxysmal dyskinesias. J Neurol 246(3):149–155

Bhatia KP, Griggs RC, Ptáček LJ (2000) Episodic movement disorders as channelopathies. Mov Disord 15(3):429–433

Caraballo R, Pavek S, Lemainque A, Gastaldi G, Echenne B, Motte J, Genton P, Cersósimo R, Humbertclaude V, Fejerman N, Monaco AP, Lathrop MG, Rochette J, Szepetowski P (2001) Linkage of benign familial infantile convulsions to chromosome 16p12-q12 suggests allelism to the infantile convulsions and choreoathetosis syndrome. Am J Hum Genet 68(3):788–794

Cuenca-Leon E, Cormand B, Thomson T, Macaya A (2002) Paroxysmal kinesigenic dyskinesia and generalized seizures: clinical and genetic analysis in a Spanish pedigree. Neuropediat 33(6):288–293

Dib C, Faure S, Fizames C, Samson D, Drouot N, Vignal A, Millasseau P, Marc S, Hazan J, Seboun E, Lathrop M, Gyapay G, Morissette J, Weissenbach J (1996) A comprehensive genetic map of the human genome based on 5246 microsatellites. Nature 380:152–154

Hattori H, Fujii T, Nigami H, Higuchi Y, Tsuji M, Hamada Y (2000) Co-segregation of benign infantile convulsions and paroxysmal kinesigenic choreoathetosis. Brain Develop 22(7):432–435

Kato N, Sadamatsu M, Kikuchi T, Niikawa N, Fukuyama Y (2006) Paroxysmal kinesigenic choreoathetosis: from first discovery in 1892 to genetic linkage with benign familial infantile convulsions. Epilepsy Res 70(Suppl 1):174–184

Lee W-L, Tay A, Ong H-T, Goh L-M, Monaco AP, Szepetowski P (1998) Association of infantile convulsions with paroxysmal dyskinesias (ICCA syndrome): confirmation of linkage to human chromosome 16p12-q12 in a Chinese family. Hum Genet 103(5):608–612

Loftus BJ, Kim UJ, Sneddon VP, Kalush F, Brandon R, Fuhrmann J, Mason T, Crosby ML, Barnstead M, Cronin L, Deslattes Mays A, Cao Y, Xu RX, Kang HL, Mitchell S, Eichler EE, Harris PC, Venter JC, Adams MD (1999) Genome duplications and other features in 12 Mb of DNA sequence from human chromosome 16p and 16q. Genomics 60(3):295–308

Nagamitsu S, Matsuishi T, Hashimoto K, Yamashita Y, Aihara M, Shimizu K, Mizuguchi M, Iwamoto H, Saitoh S, Hirano Y, Kato H, Fukuyama Y, Simada M (1999) Multicenter study of paroxysmal dyskinesias in Japan—clinical and pedigree analysis. Mov Disord 14(4):658–663

Sadamatsu M, Masui A, Sakai T, Kunugi H, Nanko S, Kato N (1999) Familial paroxysmal kinesigenic choreoathetosis: an electrophysiologic and genotypic analysis. Epilepsia 40(7):942–949

Swoboda KJ, Soong B, McKenna C, Brunt ER, Litt M, Bale JF Jr, Ashizawa T, Bennett LB, Bowcock AM, Roach ES, Gerson D, Matsuura T, Heydemann PT, Nespeca MP, Jankovic J, Leppert M, Ptáček LJ (2000) Paroxysmal kinesigenic dyskinesia and infantile convulsions: clinical and linkage studies. Neurology 55(2):224–230

Tomita H, Nagamitsu S, Wakui K, Fukushima Y, Yamada K, Sadamitsu M, Masui A, Konishi T, Matsuishi T, Aihara M, Shimizu K, Hashimoto K, Mineta M, Matsushima M, Tsujita T, Saito M, Tanaka H, Tsuji S, Takagi T, Nakamura Y, Nakano S, Kato N, Nakane Y, Niikawa N (1999) Paroxys-

mal kinesigenic choreoathetosis locus maps to chromosome 16p11.2-q12.1. Am J Hum Genet 65(6):1688–1697

Valente EM, Spacey SD, Wali GM, Bhatia KP, Dixon PH, Wood NW, Davis MB (2000) A second paroxysmal kinesigenic choreoathetosis locus (EKD2) mapping on 16q13-q22.1 indicates a family of genes which give rise to paroxysmal disorders on human chromosome 16. Brain 123(10):2040–2045

Weber YG, Berger A, Bebek N, Maier S, Karafyllakes S, Meyer N, Fukuyama Y, Halbach A, Hikel C, Kurlemann G, Neubauer B, Osawa M, Püst B, Rating D, Saito K, Stephani U, Tauer U, Lehmann-Horn F, Jurkat-Rott K, Lerche H (2004) Benign familial infantile convulsions: linkage to chromosome 16p12-q12 in 14 families. Epilepsia 45(6):601–609

J Hum Genet (2007) 52:561–564
DOI 10.1007/s10038-007-0150-5

A syndactyly type IV locus maps to 7q36

Daisuke Sato · Desheng Liang · Lingqian Wu · Qian Pan · Kun Xia · Heping Dai · Hua Wang · Gen Nishimura · Koh-Ichiro Yoshiura · Jiahui Xia · Norio Niikawa

Received: 26 March 2007 / Accepted: 2 April 2007 / Published online: 3 May 2007

Abstract Syndactyly occurs as an isolated abnormality or a part of a malformation syndrome. Syndactyly types I, II, III and V have been mapped to chromosomal regions 2q34–q36, 2q31–q32, 6q21–q23.2 and 2q31–q32, respectively, whereas syndactyly type IV (SD4) is extremely rare, and its gene localization has not yet been assigned. The SD4 manifests complete syndactyly of all fingers accompanied with polydactyly, and flexion of the fingers gives the hand a cup-shaped appearance. We performed a linkage and haplotype analysis of a Chinese pedigree with autosomal dominant, non-syndromic SD4 using a set of 406 microsatellite markers. The analysis gave the maximum two-point LOD score of 1.613 at recombination fraction of 0.00 and penetrance of 1.00. Thus, the SD4 locus in the family was likely assigned to a 17.39-cM region at a segment between markers D7S3070 and D7S559 at 7q36, although the LOD score obtained was not high enough to conclude the localization. Analysis of three candidate genes, *LMBR1*, *SHH* and *ZRS*, failed to identify any pathogenic mutations. Our gene mapping may give a clue to identify the putative SD4 gene and provide a better understanding of normal human limb development.

Keywords Syndactyly type IV · Linkage analysis · Disease gene mapping

Daisuke Sato and Desheng Liang equally contributed to this study.

D. Sato · D. Liang · L. Wu · K.-I. Yoshiura · N. Niikawa
Department of Human Genetics, Nagasaki University Graduate School of Biomedical Sciences, Nagasaki, Japan

D. Sato · D. Liang · L. Wu · K.-I. Yoshiura · N. Niikawa
Solution Oriented Research of Science and Technology (SORST), Japan Science and Technology Agency (JST), Kawaguchi, Japan

D. Sato
Department of Pediatrics, Hokkaido University Graduate School of Medicine, Sapporo, Japan

D. Liang · L. Wu (✉) · Q. Pan · K. Xia · H. Dai · J. Xia
National Laboratory of Medical Genetics, Xiangya Hospital, Central South University, 110 Xiangya Road, Changsha, Hunan 410078, China
e-mail: wulingqian@cnlmg.com

H. Wang
Women and Children's Hospital of Hunan Province, Changsha, China

G. Nishimura
Department of Radiology, Tokyo Metropolitan Kiyose Children's Hospital, Tokyo, Japan

Introduction

Syndactyly is one of the most frequent congenital limb abnormalities and occurs as an isolated anomaly or a part of a malformation syndrome. Syndactyly falls into five major types I–V based on different combinations of affected fingers and toes and showing an autosomal dominant mode of inheritance. Syndactyly type I (OMIM 185900), type II (OMIM 186000), type III (OMIM 186100) and type V (OMIM 186300) have been mapped to chromosomal regions 2q34–q36, 2q31–q32, 6q21–q23.2 and 2q31–q32, respectively. Among them, only type III syndactyly was suggested to be an allelic disorder of oculodentodigital dysplasia (ODDD, MIM 164200) that is caused by mutations in the gene for gap junction protein alpha-1 (GJA1). Genes responsible for other types of syndactyly have not been

identified. Syndactyly type IV (SD4, OMIM 186200) is extremely rare and has been reported only twice since the first description by Haas in 1940 (Gillessen-Kaesbach and Majewski 1991; Rambaud-Cousson et al. 1991). Patients with this disease have complete syndactylism of all the fingers accompanied with polydactyly and cup-shaped hands due to flexion of the fingers. The etiology of SD4 has remained unknown, and its gene localization has not yet been mapped.

We recently encountered a Chinese pedigree with autosomal dominant SD4. Herein we report on their clinical manifestations and genetic linkage study.

Materials and methods

This study was approved by the Committee for Ethical Issues on Human Genome and Gene Analysis, Nagasaki University. We ascertained a five-generation non-consanguineous Chinese family with autosomal dominant, non-syndromic syndactyly (Figs. 1, 2). The family consisted of 23 members, including 8 affected individuals (4 females and 4 males). A total of 11 family members (6 affected and 5 unaffected individuals) were available for clinical evaluations and linkage and haplotype analyses.

All the patients examined were mentally normal, but had hand and/or foot anomalies. Individuals II-2, III-2 and III-6 had bilateral complete syndactyly with flexion of fingers, cup-shaped hands, polydactyly with two additional small and non-functional fingers at the edge of both hands, six metacarpals (Fig. 2a, b) and normal feet. In addition to the hand polysyndactyly, individuals III-5 and IV-1 had foot anomalies such as seventh and eighth toes on the left and right foot, respectively, and partial cutaneous syndactyly between toes two and three. Their excess toes existed on the tibial side of both feet, and lower extremities were bent and tubby, and showed tibial hemimelia. Knee and ankle joint malformations were present in III-5 and IV-1. Radiograph of the hands and left foot of III-5 showed six metacarpals (Fig. 2g), seven metatarsals and tibial hypoplasia (Fig. 2h), leading to a diagnosis of the disease in the family as Haas type (type IV) mirror-image polydactyly of hands and feet with tibial hypoplasia. III-5 (Fig. 2c–f) also had two triphalangeal thumbs bilaterally. Individual IV-3 presented with syndactyly of fingers two to six and toes five to six, stiffness of proximal interphalangeal joints in all his fingers and two additional small and non-functional fingers bilaterally. None of the five patients showed bone fusion radiologically.

DNA samples were extracted from peripheral blood leukocytes of the 11 members of the family after obtaining written informed consents. We carried out a whole-genome search except for the chromosome X. These individuals

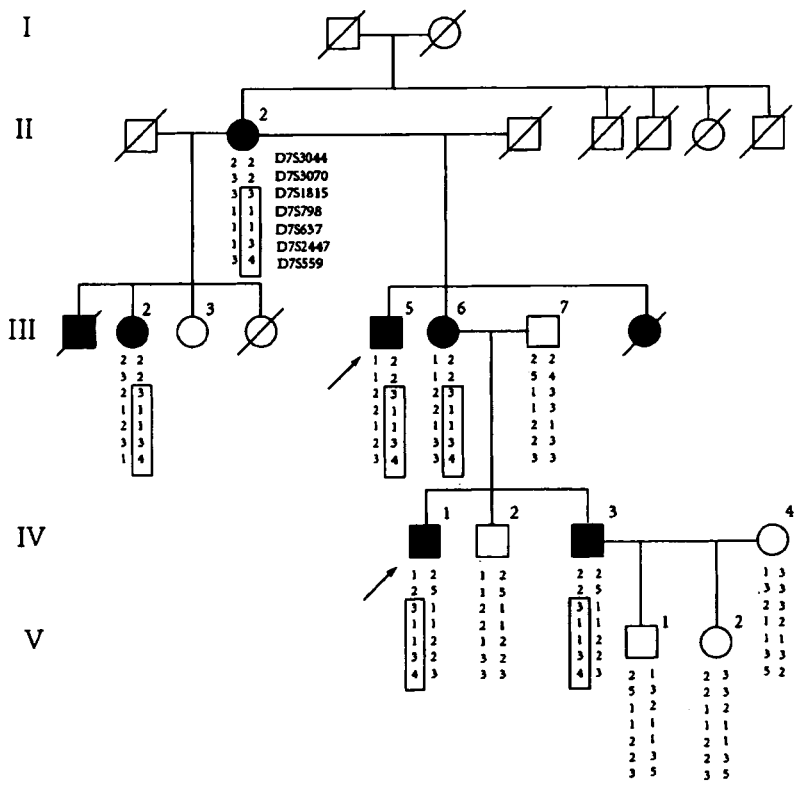

Fig. 1 Pedigree of a Chinese SD4 family with haplotypes at seven marker loci on chromosome 7. The *number in the box* depicts haplotype common to affected individuals

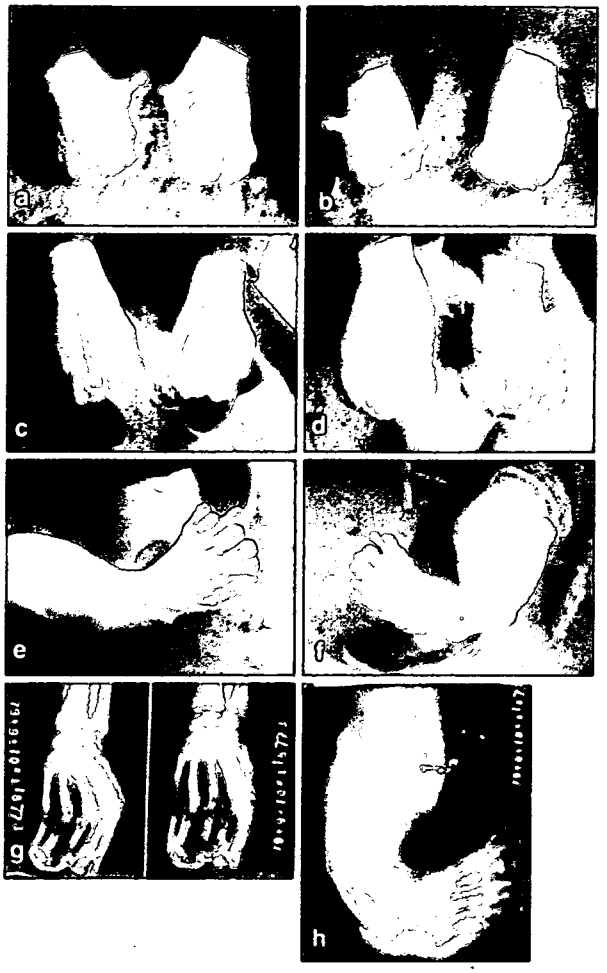

Fig. 2 Hand/foot malformations of affected individuals. **a**, **b** Polysyndactyly of fingers in III-6. **c–f** Polysyndactyly of fingers and/or toes in III-5. **g**, **h** Radiograph of hands and left leg/foot in III-5, showing six metacarpals and seven metatarsals without bone fusion, and tibial hypoplasia

were genotyped at 406 microsatellite marker loci that are distributed with an average of 10-cM intervals over the whole genome. Two-point LOD scores were calculated using the MLINK program of the FASTLINK package, assuming that the disease in the family is inherited in an autosomal dominant mode with complete penetrance (penetrance = 1.00), the disease-allele frequency is 0.001 and allele frequencies are equal at all the marker loci.

A mutation screening in three candidate genes, *LMBR1* for limb region 1 protein, *SHH* for sonic hedgehog and *ZRS* for an *SHH* regulator, was performed in six affected individuals and two unaffected members of the family. All exon and flanking intron sequences of *LMBR1* and *SHH* and a 774-bp highly conserved sequence of *ZRS* were amplified by PCR for direct sequencing. PCR conditions were set at 40 cycles of 94°C for 30 s, 62°C for 30 s and at 72°C for 45 s in a 15-μl mixture containing 1× PCR buffer with 1.5 mM $MgCl_2$, 0.2 mM each of dNTP, 1 μM each primer and 0.4 units ExTaq DNA polymerase (TaKaRa, Otsu, Japan). PCR products were treated with ExoSAP-IT (AmershamBiosciences, Piscateway, NJ), and both strands of DNA were sequenced with BigDye Terminator Sequencing kit version 3.1 according to the supplied protocol (AppliedBiosystems, Foster City, CA). The reaction mixture was purified using Sephadex G-50 superfine (AmershamBiosciences) and analyzed on the ABI Genetic Analyzer 3100 (AppliedBiosystems) with the Sequence-Analysis software (AppliedBiosystems) and aligned with the AutoAssembler version2.1.1 software (AppliedBiosystems) to find DNA alterations.

Results and discussion

The disease in the Chinese family was clinically diagnosed as syndactyly type IV (SD4), because one (III-5) of the affected members had complete syndactylism of all fingers and toes accompanied with polydactyly. Flexion of fingers together with cutaneous syndactyly gave his hands a cup-shaped appearance. SD4 in the family was inherited as an autosomal dominant mode as was reported in the family with SD4 (Gillessen-Kaesbach and Majewski 1991; Rambaud-Cousson et al. 1991).

At an initial genotyping at the 406 marker loci, only seven members [five affected and two unaffected members (II-2, III-2 and 5–7, and IV-2 and 3)] were available. We obtained a possible linkage of the disease locus to five markers (*D2S2152*, *D7S559*, *D12S1052*, *D16S3039* and *D17S1822*) on chromosomes 2, 7, 12, 16 and 17 with LOD scores higher than 1.00. However, haplotype analysis excluded four of the five loci and retained *D7S559* as a candidate region for SD4 at 7q36.3. We then performed a second analysis by the use of more markers around 7q36.3 and by adding four more members (one patient IV-1 and three unaffected members IV-4, V-1 and V-2) who participated in the study later. The maximum two-point LOD score within the locus was 1.613 at recombination fraction of 0.00 and penetrance of 1.00 (Table 1). Haplotype analysis showed that all the six affected members had the same haplotype "3-1-1-3-4" for five marker loci, D7S1815, D7S798, D7S637, D7S2447 and D7S559 (Fig. 1). From these findings, it is most likely that SD4 in the Chinese family was assigned to a 17.39-cM region at 7q36, although the LOD score obtained was not high enough to conclude a concrete linkage. Direct sequencing of patients' DNA for exon and flanking intron sequences of *LMBR1* and *SHH* and the conserved sequence of *ZRS* revealed no pathogenic mutation.

To a similar region where we assigned a SD4 locus, several forms of limb abnormalities have been mapped.

Table 1 Two-point LOD score of chromosome 7q markers at various recombination fractions

Marker	Position (cM)	LOD score at theta (penetrance = 1.00)						
		0.00	0.05	0.10	0.15	0.20	0.25	0.30
D7S3044	153.7	−2.75	−0.480	−0.225	−0.096	−0.021	0.024	0.047
D7S3070	165.6	0.68	0.714	0.700	0.657	0.594	0.517	0.430
D7S1815	167.1	1.380	1.276	1.166	1.050	0.928	0.798	0.660
D7S798	169.9	0.861	0.796	0.728	0.657	0.581	0.500	0.415
D7S637	174.0	0.519	0.479	0.437	0.393	0.347	0.298	0.246
D7S2447	175.5	1.192	1.013	0.900	0.784	0.663	0.540	0.415
D7S559	183.0	1.613	1.446	1.271	1.090	0.902	0.712	0.526

They include preaxial polydactyly (Hing et al. 1995; Heus et al. 1999; Zguricas et al. 1999), complex polysyndactyly (Tsukurov et al. 1994), triphalangeal thumb (Heutink et al. 1994; Radhakrishna et al. 1996; Balci et al. 1999) and acheiropodia (Ianakiev et al. 2001). Among genes in the region, *LMBR1*, *SHH* and *ZRS* merit comments. It was shown that five point mutations residing in the highly conserved sequence of *ZRS* were associated with congenital preaxial polydactyly (Lettice et al. 2003; Gurnett et al. 2007), mutations in the chicken *Lmbr1* are linked to chicken polydactyly (Huang et al. 2006), and *Shh* was responsible for the digit duplication activity in chick embryos (Riddle et al. 1993). Unfortunately, we failed to identify any pathogenic mutations of these genes in the SD4 patients from the Chinese family.

In conclusion, we have mapped the SD4 locus in the Chinese family to 7q36. This may become a clue to identify the gene responsible for this rare disease and provide a better understanding of normal human limb development.

Acknowledgments We are grateful to the patients and relatives for their participation in this study. N. Niikawa was supported in part by a Grant-in-Aid for Scientific Research (Priority Areas for Applied Genomics, no. 17019055) from the Ministry of Education, Culture, Sports, Science and Technology of Japan and by SORST from the Japan Science and Technology Agency (JST). L. Wu was supported by the Research Grant (30571201) from National Natural Science Foundation of China.

Conflict of interest The authors of this manuscript declare that they have no competing interests.

References

Balci S, Demirtas M, Civelek B, Piskin M, Sensoz O, Akarsu AN (1999) Phenotypic variability of triphalangeal thumb-polysyndactyly syndrome linked to chromosome 7q36. Am J Med Genet 87:399–406

Gillessen-Kaesbach G, Majewski F (1991) Bilateral complete polysyndactyly (type IV Haas). Am J Med Genet 38:29–31

Gurnett CA, Bowcock AM, Dietz FR,Morcuende JA, Murray JC, Dobbs MB (2007) Two novel point mutations in the long-range SHH enhancer in three families with triphalangeal thumb and preaxial polydactyly. Am J Med Genet 143:27–32

Haas SL (1940) Bilateral complete syndactylism of all fingers. Am J Surg:363–366

Heus HC, Hing A, van Baren MJ, Joosse M, Breedveld GJ, Wang JC, Burgess A, Donnis-Keller H, Berglund C, Zguricas J, Scherer SW, Rommens JM, Oostra BA, Heutink P (1999) A physical and transcriptional map of the preaxial polydactyly locus on chromosome 7q36. Genomics 57:342–351

Heutink P, Zguricas J, van Oosterhout L, Breedveld GJ, Testers L, Sandkuijl LA, Snijders PJLM, Weissenbach J, Lindhout D, Hovius SER, Oostra BA (1994) The gene for triphalangeal thumb maps to the subtelomeric region of chromosome 7q. Nat Genet 6:287–291

Hing AV, Helms C, Slaugh R, Burgess A, Wang JC, Herman T, Dowton SB, Donis-Keller H (1995) Linkage of preaxial polydactyly type 2 to 7q36. Am J Med Genet 58:128–135

Huang YQ, Deng XM, Du ZQ, Qiu X, Du X, Chen W, Morisson M, Leroux S, Ponce de Leon FA, Da Y, Li N (2006) Single nucleotide polymorphisms in the chicken *Lmbr1* gene are associated with chicken polydactyly. Gene 374:10–18

Ianakiev P, van Baren MJ, Daly MJ, Toledo SPA, Cavalcanti MG, Correa Neto J, Lemos Silveira E, Freire-Maia A, Heutink P, Kilpatrick MW, Tsipouras P (2001) Acheiropodia is caused by a genomic deletion in c7orf2, the human orthologue of the *Lmbr1* gene. Am J Hum Genet 68:38–45

Lettice LA, Heaney SJH, Purdie LA, Li L, de Beer P, Oostra BA, Goode D, Elgar G, Hill RE, de Graaff E (2003) A long-range *Shh* enhancer regulates expression in the developing limb and fin and is associated with preaxial polydactyly. Hum Mol Genet 12:1725–1735

Radhakrishna U, Blouin JL, Solanki JV, Dhoriani GM, Antonarakis SE (1996) An antosomal dominant triphalangeal thumb: polysyndactyly syndrome with variable expression in a large Indian family maps to 7q36. Am J Med Genet 66:209–215

Rambaud-Cousson A, Dudin AA, Zuaiter AS, Thalji A (1991) Syndactyly type IV/hexadactyly of feet associated with unilateral absence of the tibia. Am J Med Genet 40:144–145

Riddle RD, Johnson RL, Laufer E, Tabin C (1993) Sonic hedgehog mediates the polarizing activity of the ZPA. Cell 75:1401–1416

Tsukurov O, Boehmer A, Flynn J, Nicolai JP, Hamel BCJ, Traill S, Zaleske D, Mankin HJ, Yeon H, Ho C, Tabin C, Seidman JG, Seidman C (1994) A complex bilateral polysyndactyly disease locus maps to chromosome 7q36. Nat Genet 6:282–286

Zguricas J, Heus H, Morales-Peralta E, Breedveld G, Kuyt B, Mumcu EF, Bakker W, Akarsu N, Kay SPJ, Hovius SER, Heredero-Baute L, Oostra BA, Heutink P (1999) Clinical and genetic studies on 12 preaxial polydactyly families and refinement of the localisation of the gene responsible to a 1.9 cM region on chromosome 7q36. J Med Genet 36:32–40

Quantitative Structure–Activity Relationship Analysis and Molecular Dynamics Simulation To Functionally Validate Nonsynonymous Polymorphisms of Human ABC Transporter ABCB1 (P-Glycoprotein/MDR1)

Aki Sakurai, Yuko Onishi, Hiroyuki Hirano, Michel Seigneuret, Kazuya Obanayama, Gunwoo Kim, Ei Leen Liew, Toshiyuki Sakaeda, Koh-ichiro Yoshiura, Norio Niikawa, Minoru Sakurai, and Toshihisa Ishikawa

Department of Biomolecular Engineering, Graduate School of Bioscience and Biotechnology, Tokyo Institute of Technology, Yokohama, Japan, Institut Cochin, Departement de Biologie Cellulaire, CNRS (UMR 8104), INSERM (U567), Université Paris 5, Paris, France, Center for Integrative Education of Pharmacy Frontier, Graduate School of Pharmaceutical Sciences, Kyoto University, Kyoto, Japan, Department of Human Genetics, Nagasaki University Graduate School of Biomedical Sciences, Nagasaki, Japan, and CREST, Japan Science and Technology, Kawaguchi, Japan

Biochemistry®

Reprinted from
Volume 46, Number 26, Pages 7678–7693

Articles

Quantitative Structure−Activity Relationship Analysis and Molecular Dynamics Simulation To Functionally Validate Nonsynonymous Polymorphisms of Human ABC Transporter ABCB1 (P-Glycoprotein/MDR1)†

Aki Sakurai,‡ Yuko Onishi,‡ Hiroyuki Hirano,‡ Michel Seigneuret,§ Kazuya Obanayama,‡ Gunwoo Kim,‡ Ei Leen Liew,‡ Toshiyuki Sakaeda,|| Koh-ichiro Yoshiura,⊥,# Norio Niikawa,⊥,# Minoru Sakurai,‡ and Toshihisa Ishikawa*,‡

Department of Biomolecular Engineering, Graduate School of Bioscience and Biotechnology, Tokyo Institute of Technology, Yokohama, Japan, Institut Cochin, Departement de Biologie Cellulaire, CNRS (UMR 8104), INSERM (U567), Université Paris 5, Paris, France, Center for Integrative Education of Pharmacy Frontier, Graduate School of Pharmaceutical Sciences, Kyoto University, Kyoto, Japan, Department of Human Genetics, Nagasaki University Graduate School of Biomedical Sciences, Nagasaki, Japan, and CREST, Japan Science and Technology, Kawaguchi, Japan

Received January 13, 2007; Revised Manuscript Received April 28, 2007

ABSTRACT: Several preclinical and clinical studies suggest the importance of naturally occurring polymorphisms of drug transporters in the individual difference of drug response. To functionally validate the nonsynonymous polymorphisms of ABCB1 (P-glycoprotein/MDR1) in vitro, we generated SNP variant forms (i.e., S400N, R492C, R669C, I849M, A893P, A893S, A893T, M986V, A999T, P1051A, and G1063A) and expressed them in Sf9 cells. The kinetic properties (K_m and V_{max}) of those variants were analyzed by measuring the ATPase activity to obtain the ATPase profile for each variant toward structurally unrelated substrates. On the basis of the experimental data, we determined the substrate specificity of ABCB1 WT and its variants by the quantitative structure−activity relationship (QSAR) analysis method. While several SNP variants appeared to influence the substrate specificity of ABCB1, the nonsynonymous polymorphisms of 2677G > T, A, or C at amino acid position 893 (Ala > Ser, Thr, or Pro) have great impacts on both the activity and the substrate specificity of ABCB1. The A893P variant (2677G > C), a rare mutation, exhibited markedly high activity of ATPase toward different test compounds. Molecular dynamics (MD) simulation based on a three-dimensional structural model of human ABCB1 revealed that multiple kinks are formed in the intracellular loop between transmembrane domains 10 and 11 of the A893P variant (2677G > C) protein. The polymorphisms of 2677G, 2677T, and 2677A exhibit wide ethnic differences in the allele frequency, and these nonsynonymous polymorphisms are suggested to be clinically important because of their altered ATPase activity and substrate specificity toward different drugs.

Pharmacogenomics dealing with heredity and response to drugs is a part of science that attempts to explain the variability of one or another drug response and to search for the genetic basis of such variations or differences. As a means to implementing personalized medicine based on pharmacogenomic data, it is critically important to understand the molecular mechanisms underlying interindividual differences in the drug response, namely, pharmacological effect vs side effect. The occurrence of individual variations in the drug response may involve many different causes, for example, genetic variations and/or expression levels of drug target molecules, including membrane receptors, nuclear receptors, signal transduction components, and enzymes, as well as those of drug metabolizing enzymes and, importantly, drug transporters.

Human ABCB1[1] (P-glycoprotein or MDR1) was identified because of its overexpression in cultured cancer cells associated with an acquired cross-resistance to multiple anticancer drugs (*1*, *2*). ABCB1 is expressed not only in cancer cells but also in many normal tissues. For example, it is located in the apical domain of the enterocytes of the gastrointestinal tract (jejunum and duodenum) and limits the uptake and absorption of drugs and other substrates from the intestine into the systemic circulation by excreting

† This study was supported by the NEDO International Joint Research Grant program "International standardization of functional analysis technology for genetic polymorphisms of drug transporters" and a research grant (14370754) from the Japanese Society for the Promotion of Science.

* Corresponding author. Phone: +81-45-924-5800. Fax: +81-45-924-5838. E-mail: tishikaw@bio.titech.ac.jp.

‡ Tokyo Institute of Technology.

§ Université Paris 5.

|| Kyoto University.

⊥ Nagasaki University Graduate School of Biomedical Sciences.

CREST.

10.1021/bi700330b CCC: $37.00
Published on Web 06/09/2007

substrates into the gastrointestinal tract. In addition, ABCB1 is expressed in the endothelial cells lining the small vessels of the human cortex, in which the transporter appears to be concentrated within the luminal cellular compartment. The expression of ABCB1 on the luminal membrane of capillary endothelial cells of the brain restricts drug distribution into the central nervous system (*3*, *4*). This function of ABCB1 appears to be very important for protecting the central nervous system from attack by toxic compounds.

To date, genetic variations of the human *ABCB1* gene have been most extensively studied (*5*). Hitherto, more than 50 SNPs and several insertion/deletion polymorphisms in the *ABCB1* gene have been reported (*5*−*24*). Preclinical and clinical studies have provided evidence for naturally occurring polymorphisms in ABCB1 and their effects on drug absorption, distribution, and elimination (*25*). Hoffmeyer et al. reported multiple polymorphisms in the *ABCB1* gene (*6*). One of those mutations in particular, a C-to-T variant at position 3435 in exon 26 of the *ABCB1* gene, was reportedly correlated with ABCB1 expression and function, whereas an association of the 3435C > T polymorphism with ABCB1 protein expression and function remains controversial. It has been suggested that the 2677G > T/3435C > T haplotype is of clinical importance (*8*, *10*, *16*, *26*). In this regard, Kimchi-Sarfaty et al. have most recently reported that the haplotype polymorphism of 1236C > T/2677G > T/3435C > T might change the substrate specificity of ABCB1 (*27*). Currently available reports as well as the NCBI dbSNP database show a triallelic polymorphism of ABCB1 (2677G > T/A) and one rare mutation (2677G > C). At present, however, information is still limited regarding the functional impact of the genetic polymorphisms in the *ABCB1* gene. Detailed functional analysis in vitro may provide clear insight into the biochemical and therapeutic significance of genetic polymorphisms.

In the present study, we have undertaken an in vitro quantitative analysis to precisely evaluate functional changes associated with genetic polymorphisms of ABCB1. For this purpose, ABCB1 cDNA cloned from a human liver cDNA library was prepared, and several variant forms (i.e., S400N, R492C, R669C, I849M, A893S, A893T, A893P, M986V, A999T, P1051A, and G1063A) were generated by site-directed mutagenesis. We have functionally evaluated those variants by using the newly developed quantitative structure−activity relationship (QSAR) analysis technique. Furthermore,

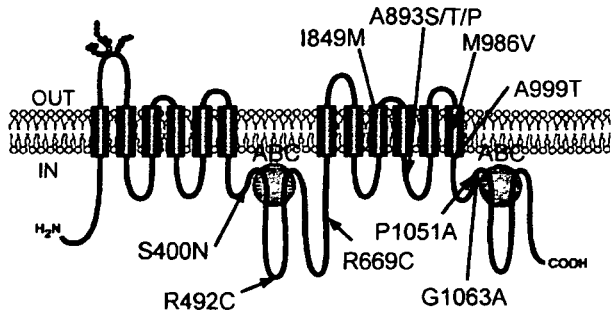

FIGURE 1: Schematic illustration of the human ABCB1 protein and positions of nonsynonymous SNPs that were functionally analyzed in the present study. SNP data were obtained from the NCBI dbSNP database and recent publications: S400N (*6*, *7*, *29*, *31*); R492C (*7*); R669C (*16*); I849M (*16*); A893P (NCBI dbSNP, rs2032582); A893S (*8*, *16*, *23*, *29*−*31*); A893T (*8*, *16*, *23*, *29*−*31*); M986V (*30*); A999T (*28*); P1051A (*16*); G1063A (NCBI dbSNP, rs2707944). ATP-binding cassettes are indicated by ABC.

based on a putative three-dimensional structural model of human ABCB1, molecular dynamics (MD) simulation was carried out to gain more insight into the impact of nonsynonymous polymorphisms on structural changes that may affect the ATPase activity of ABCB1. Evidence is provided herein to show that nonsynonymous polymorphisms (2677G > T, A, or C) at amino acid position 893 (Ala > Ser, Thr, or Pro) have a great impact on both the activity and the substrate specificity of ABCB1.

EXPERIMENTAL PROCEDURES

Chemicals and Biochemicals. The following compounds and therapeutic drugs were purchased from the commercial sources indicated in parentheses: ATP magnesium salt, sodium *o*-vanadate, epinephrine, norepinephrine, γ-aminobutyric acid (GABA), serotonin, melatonin, nifedipine, bepridil, fendiline, prenylamine, nicardipine, dexamethasone, prednisolone, cortisone, pinacidil, acetylsalicylic acid, indomethacin, acemetacin, ibuprofen, naproxen, mepirizole, vinblastine, etoposide, daunorubicin, paclitaxel, doxorubicin, 5-fluorouracil, quinidine, *p*-aminohippuric acid (PAH), penicillin G (benzylpenicillin), and novobiocin (Sigma-Aldrich Co., St. Louis, MO); glutamic acid, dopamine, histamine, verapamil, diltiazem, betamethasone, nicorandil, actinomycin D, and methotrexate (Wako Pure Chemical Industries, Ltd., Osaka, Japan); glycine, Tris, HEPES, EGTA, and EDTA (Nacalai Tesque, Inc., Kyoto, Japan); tacrolimus (Calbiochem, Darmstadt, Germany). All other chemicals were of analytical grade.

SNP Data on Nonsynonymous Polymorphisms of the Human ABCB1 Gene. SNP data on polymorphisms of the *ABCB1* gene were obtained from the NCBI dbSNP database (http://www.ncbi.nlm.nih.gov/SNP/snp_ref.cgi?locusId=5243) and recent publications (*6*−*8*, *16*, *23*, *28*−31). Figure 1 illustrates the positions of the nonsynonymous polymorphisms of ABCB1 that were functionally analyzed in the present study.

Preparation of Plasmids Carrying ABCB1 Variants. Wild-type (WT) ABCB1 cDNA (NCBI NM_000927.3) was inserted into the pFastBac1 plasmid as described previously (*32*). Nonsynonymous SNP variants were generated by using the QuikChange site-directed mutagenesis kit (Stratagene, La Jolla, CA). Polymerase chain reaction (PCR) was carried

[1] Abbreviations: ABC, ATP-binding cassette; cDNA, complementary DNA; CFC, chemical fragmentation code; ATP, adenosine triphosphate; EDTA, ethylenediaminetetraacetic acid; AMBER, assisted model building and energy refinement; EGTA, ethylene glycol bis(β-aminoethyl ether)-*N*,*N*,*N*′,*N*′-tetraacetic acid; FCS, fetal calf serum; GABA, γ-aminobutyric acid; HEPES, 2-[4-(2-hydroxyethyl)-1-piperazinyl]-ethanesulfonic acid; HRP, horseradish peroxidase; IgG, immunoglobulin G; K_m, Michaelis−Menten constant; MD, molecular dynamics; MDR, multidrug resistance; MES, 2-(*N*-morpholino)ethanesulfonic acid; NCBI, National Center for Biotechnology Information; NSAID, nonsteroidal antiinflammatory drug; PAH, *p*-aminohippuric acid; PBS, phosphate-buffered saline; PCR, polymerase chain reaction; QSAR, quantitative structure−activity relationship; RMSF, root-mean-square fluctuation; SAR, structure−activity relationship; SDS−PAGE, sodium dodecyl sulfate−polyacrylamide gel electrophoresis; SD, standard deviation; SNP, single nucleotide polymorphism; TM, transmembrane domain; Tris, tris(hydroxymethyl)aminomethane; TBS, Tris-buffered saline; TTBS, Tris-buffered saline containing 0.05% (v/v) Tween 20; V_{max}, maximum velocity; WT, wild type.

Table 1: Data on Oligonucleotide Primers Used for Site-Directed Mutagenesis and Experimental Conditions[a]

SNP						
amino acid	cDNA	F/R primers	primer sequence (5′ → 3′)	primer length (bases)	% GC	T_m (°C)
S400N	1199G > A	F	CAGAAATGTTCACTTCAATTACCCATCTCGAAAAG	35	36.5	77.2
		R	CTTTTCGAGATGGGTAATTGAAGTGAACATTTCTG	35	36.5	77.2
R492C	1474C > T	F	TGAAAACATTCGCTATGGCTGTGAAAATGTCACCATGG	38	42.1	81.0
		R	CCATGGTGACATTTTCACAGCCATAGCGAATGTTTTCA	38	42.1	81.0
R669C	2005C > T	F	TCTAATAAGAAAAAGATCAACTTGTAGGAGTGTCCGTGGATC	42	37.9	80.9
		R	GATCCACGGACACTCCTACAAGTTGATCTTTTTCTTATTAGA	42	37.9	80.9
I849M	2547A > G	F	GGGACAGGAATAATTATGTCCTTCATCTATGGTTGGCA	38	34.5	77.9
		R	TGCCAACCATAGATGAAGGACATAATTATTCCTGTCCC	38	34.5	77.9
A893P	2677G > C	F	AGAAAGAACTAGAAGGTCCTGGGAAGATCGCTAC	34	47.1	80.9
		R	GTAGCGATCTTCCCAGGACCTTCTAGTTCTTTCT	34	47.1	80.9
A893S	2677G > T	F	GAAAGAACTAGAAGGTTCTGGGAAGATCGCTAC	33	45.4	79.6
		R	GTAGCGATCTTCCCAGAACCTTCTAGTTCTTTC	33	45.4	79.6
A893T	2677G > A	F	GAAAGAACTAGAAGGTACTGGGAAGATCGCTAC	33	45.4	79.6
		R	GTAGCGATCTTCCCAGTACCTTCTAGTTCTTTC	33	45.4	79.6
M986V	2956A > G	F	GTCTTTGGTGCCGTGGCCGTGGGGC	25	73.8	84.7
		R	GCCCCACGGCCACGGCACCAAAGAC	25	73.8	84.7
A999T	2995G > A	F	GTTCATTTGCTCCTGACTATACCAAAGCCAAAATATCAGCAG	42	40.5	82.0
		R	CTGCTGATATTTTGGCTTTGGTATAGTCAGGAGCAAATGAAC	42	40.5	82.0
P1051A	3151C > G	F	CGACCGGACATCGCAGTGCTTCAGGG	26	60.0	80.1
		R	CCCTGAAGCACTGCGATGTCCGGTCG	26	60.0	80.1
G1063A	3188G > C	F	GAGGTGAAGAAGGCCCAGACGCTGGCTC	28	64.3	83.7
		R	GAGCCAGCGTCTGGGCCTTCTTCACCTC	28	64.3	83.7

[a] F, forward; R, reverse. Sites of mutagenesis are indicated by underbars. The % GC indicates the percentage of guanine and cytosine contents in the PCR primers. T_m shows the melting temperature for each PCR primer set.

out in an iCycler (Bio-Rad Laboratories, Inc., Hercules, CA) by using PfuTurbo DNA polymerase, the ABCB1-pFastBac1 plasmid, and specific primers (see Table 1 for primer sequences). The PCR was initiated with incubation at 94 °C for 2 min and then followed by 12 cycles of reactions at 94 °C for 30 s, at 55 °C for 30 s, and at 68 °C for 18 min. After the PCR, the reaction mixture was incubated with *Dpn*I endonuclease at 37 °C for 1 h to digest the original template plasmid. Each variant cDNA generated in the pFastBac1 plasmid was subjected to nucleotide sequence analysis (Hitachi, Ltd., Tokyo, Japan).

Expression of ABCB1 WT and SNP Variants in Insect Sf9 Cells. Competent DH10Bac *Escherichia coli* cells were transformed by the variant ABCB1 plasmids. Then, the variant ABCB1 cDNA was transposed into the bacmid, which is the baculovirus' genome, in DH10Bac cells with the help of a helper plasmid. The recombinant bacmid was isolated and purified by using a QIAprep Spin Miniprep kit (Qiagen K.K., Tokyo, Japan).

Insect *Spodoptera frugiperda* (Sf9) cells were grown in EX-CELL 420 medium (JRH Biosciences, Inc., Lenexa, KS) supplemented with 1% (v/v) fetal calf serum (FCS) and 1% (v/v) antibiotic-antimycotic (Invitrogen Co., Carlsbad, CA) with gentle shaking at 27 °C. Sf9 cells were then transfected with the ABCB1-recombinant bacmid in the presence of Cellfectin reagent (Invitrogen Co., Carlsbad, CA) according to the manufacturer's protocol. Ninety-six hours after the transfection, the culture medium containing recombinant baculoviruses was harvested by centrifugation. To amplify the recombinant baculoviruses, Sf9 cells were further infected with the harvested virus and maintained for 72 h, after which the culture medium was harvested by centrifugation. This process was repeated three times.

To detect ABCB1 or its variants expressed in Sf9 cells, samples of the culture medium were taken, and 2.0×10^6 cells in the medium were rinsed with phosphate-buffered saline (PBS) and collected by centrifugation. A 1 mL syringe with a 27 G needle was then used to homogenize the cells in 100 μL of cell lysis buffer containing 50 mM Tris-HCl (pH 7.4), 1% (v/v) Triton X-100, 1 mM dithiothreitol, and protease inhibitor cocktail (Nacalai Tesque, Inc., Kyoto, Japan). Subsequently, the homogenate was centrifuged at 800*g* at 4 °C for 5 min. The resulting supernatant was collected, and the protein concentration was measured with a BCA protein assay reagent kit (Pierce Biotechnology, Inc., Rockford, IL).

Immunoblot Analysis for Detection of ABCB1 WT and Its Variants. The supernatant (10 μg of protein) was subjected to sodium dodecyl sulfate–polyacrylamide gel electrophoresis (SDS–PAGE). The separated proteins were subsequently transferred to a nitrocellulose membrane (Hybond ECL; Amersham Biosciences Corp., Piscataway, NJ). Following an incubation with 5% skim milk in Tris-buffered saline (TBS) at room temperature for 60 min, the nitrocellulose membrane was incubated with ABCB1-specific monoclonal antibody C219 (1:100 dilution; Calbiochem, Darmstadt, Germany) in Tris-buffered saline containing 0.05% (v/v) Tween 20 (TTBS) at room temperature for 90 min. Afterward, the nitrocellulose membrane was incubated with an anti-mouse IgG–horseradish peroxidase (HRP) conjugate (Cell Signaling Technology, Beverly, MA) diluted to 1:3000 in TTBS. HRP-dependent luminescence was developed by using the Western Lightning Western Blot Chemiluminescence Reagent Plus kit (Perkin-Elmer Life Sciences, Inc., Boston, MA). The chemiluminescence was detected in a Lumino Imaging Analyzer FAS-1000 (Toyobo Co., Ltd., Osaka, Japan), and the intensity was quantified by using a Gel Pro Analyzer v-3.1 (Toyobo Co., Ltd., Osaka, Japan).

Preparation of Plasma Membrane. Sf9 cells (1×10^6 cells/mL) were infected with the ABCB1-recombinant baculovirus. Plasma membrane fractions were prepared from Sf9 cells as described previously (*32*). Briefly, seventy-two hours after

infection, the cells were collected by centrifugation at 300*g* at 4 °C for 5 min and rinsed with PBS. The cells were homogenized with a Potter-Elvehjem homogenizer in hypotonic buffer (0.5 mM Tris−HEPES, 0.1 mM EGTA, pH 7.4). After centrifugation at 9100*g* at 4 °C for 10 min, the supernatants were pooled and centrifuged at 100000*g* at 4 °C for 30 min. The resulting precipitate was homogenized with a Potter-Elvehjem homogenizer in 10 mL of 0.25 M sucrose and 10 mM Tris−HEPES solution (pH 7.4). This mixture was layered over a 40% (w/v) sucrose solution containing 10 mM Tris−HEPES (pH 7.4) and then centrifuged at 100000*g* at 4 °C for 30 min. The turbid layer at the interface was collected and mixed with 10 mL of 0.25 M sucrose solution containing 10 mM Tris−HEPES (pH 7.4). The mixture was centrifuged at 100000*g* at 4 °C for 30 min. The resulting precipitate was suspended in a small volume of 0.25 M sucrose solution containing 10 mM Tris−HEPES (pH 7.4).

Measurement of ABCB1 ATPase Activity. The ATPase activity of ABCB1 and its variants in the Sf9 plasma membrane fraction was measured in the presence of various test compounds in 96-well plates, as described previously (*32*, *33*). Cell membranes (2 μg of protein per well) were suspended in 10 μL of the incubation medium containing 50 mM Tris−MES (pH 6.8), 2 mM EGTA, 2 mM dithiothreitol, 50 mM potassium chloride, 5 mM sodium azide, and 2 mM ouabain (*33*). This medium was mixed with 10 μL of a test compound solution and then preincubated at 37 °C for 3 min. The ATPase reaction was started by adding 20 μL of 4 mM ATP/Mg solution to the reaction mixture, and the incubation was maintained at 37 °C for 30 min. The reaction was stopped by the addition of 20 μL of 5% trichloroacetic acid followed by 42 μL of solution A (2 M hydrochloric acid:0.1 M sodium molybdate = 4:3) and 18 μL of solution B [0.084% (w/v) malachite green in 1% (w/v) polyvinyl alcohol solution]. Thereafter, 120 μL of solution C [7.8% (v/v) sulfuric acid] was added to the mixture. These mixing processes were automatically carried out in a HALCS-I system (BioTec Co. Ltd., Tokyo, Japan). One hour after incubation at room temperature, the absorbance of each reaction mixture in the 96-well plates was photometrically measured at a wavelength of 630 nm in a Multiskan JX system (Dainippon Pharmaceuticals Co., Osaka, Japan). The amount of liberated phosphate was quantified on the basis of the calibration line established with inorganic phosphate standards. Throughout this study, we measured drug-stimulated ATPase activities (vanadate-sensitive) that were observed in ABCB1-expressing membrane preparations (see Results).

QSAR Analysis Using Chemical Fragmentation Codes. To perform the QSAR analysis for the functional validation of nonsynonymous polymorphisms of ABCB1 in this study, we generated the chemical fragmentation codes (CFCs) of all of the test compounds by using the Markush TOPFRAG program (http://scientific.thomson.com/support/patents/patinf/terms/). The CFCs are a set of alphanumeric symbols, each representing a fragment of a chemical structure. The Markush TOPFRAG program is a tool for searching the chemical structures and structure information in Derwent's online databases (http://www.biobyte.com/bb/prod/40manual.pdf). In the present study, we have formulated the extent of drug-stimulated ATPase activity of ABCB1 as a linear combination of CFCs, each of which was weighted by the corresponding coefficient, $C(i)$, as follows: where the symbol (i)

$$\text{drug-stimulated ATPase activity of ABCB1} = \sum C(i) \times \text{score (i)} + \text{constant}$$

designates a specific CFC. The "score" means the presence (≥ 1) or absence (0) of the corresponding CFC in the chemical structure of a test compound. On the basis of the CFCs thus obtained and in comparison with the observed inhibition of transport activity for each test compound, we have calculated chemical fragmentation coefficients, $C(i)$, by multiple linear regression analysis, as described previously (*34*).

Homology Modeling of the ABCB1 3D Structure. An alignment of the sequence of human ABCB1 with twice that of the *Staphylococcus aureus* Sav1866 monomer was generated automatically with the ClustalX program (*35*) and optimized manually. Ambiguities occurred only in the alignment of the first, fifth, and sixth TM regions of each transporter half. These were resolved in each case by carrying out homology modeling with the different possible alignments and choosing the one that yielded no polar residue at the surface of the hydrophobic TM region of the final structure. The final alignment corresponds respectively to a 29% and 27% identity of the ABCB1 first and second transporter half with the Sav1866 monomer.

Homology modeling was performed with Modeller 7.7 (*36*). The first stage of modeling was done with the "model" routine using the Sav1866 dimer crystal structure (ref *37*; PDB code 2HYD) as template. The 627−693 linker region of ABCB1 was not considered in the present study since it apparently bears no structural relevance to function apart from a flexibility requirement (*38*). Twenty-five structures were generated, and one was chosen, corresponding to a low value of the Modeller convergence function and to stereochemically adequate bond angles, bond lengths, and backbone dihedrals. In a second stage, the Modeller 7.7 "loop" routine (*39*) was used to optimize the conformations of nonaligned loops. All loops were optimized together. Fifty structures were generated, and one was chosen, corresponding to the major conformation of the large first extracellular loop and to an overall adequate bond and angle stereochemistry of all modeled loops. This final structure was quality-checked with WHAT IF (*40*) and PROCHECK (*41*). Ramachandran analysis indicated that 99.4% of the residues' backbone dihedrals were in allowed regions. Bond angle and length Z-scores were found to be satisfactory, and only minor steric clashes (<0.36 Å) were detected.

MD Simulation. The initial three-dimensional structure of each variant protein (A893S, A893T, or A893P) was deduced from the ABCB1 structure template by using the LEAP module in the AMBER (assisted model building and energy refinement) simulation package. MD simulation was performed for those three-dimensional structure models by using the AMBER version 8.0 simulation program that had been developed by Case et al. (*42*). In the MD simulation, we used the force field parameter set of ff03 and represented the solvent as a generalized Born solvent model (*43*). Briefly, all atoms in each system were first minimized for 12000 steps by using the steepest descent algorithm to remove close contacts and to relax the system. Next, each system was

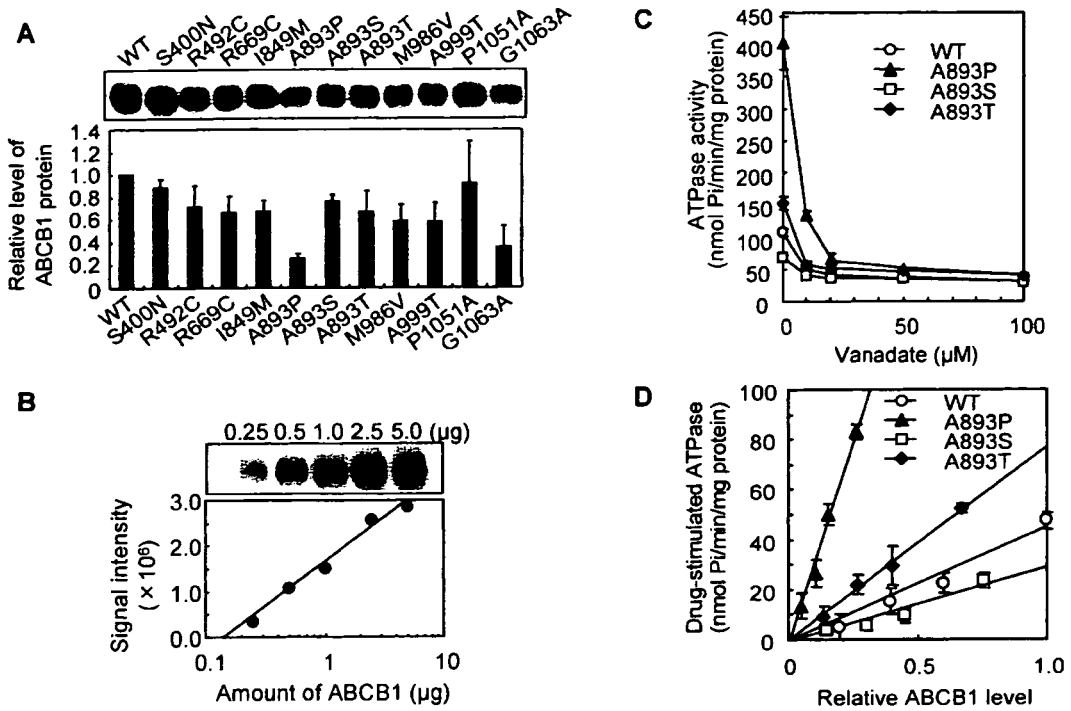

FIGURE 2: Immunoblotting detection of ABCB1 WT and variants expressed in plasma membranes. (A) Protein levels of ABCB1 WT and variants expressed in plasma membranes prepared from Sf9 cells. ABCB1 was detected by immunoblotting as described in Experimental Procedures. Proteins in Sf9 plasma membranes (2.5 μg each) were separated by 7.5% SDS–PAGE. ABCB1 WT and variants were detected by specific monoclonal antibody C219 and the anti-mouse IgG–HRP conjugate. HRP-dependent chemiluminescence was detected in a Lumino Imaging Analyzer FAS-1000. The relative levels of ABCB1 WT and variant proteins in the plasma membrane were calculated from the calibration curve of the ABCB1 protein level vs the signal intensity. Data are expressed as mean values ± SD (n = 3). (B) Relationship between the ABCB1 protein level and the intensity of chemiluminescence. Plasma membranes (0, 0.25, 0.5, 1.0, 2.0, and 5.0 μg of protein) of Sf9/ABCB1 WT cells were analyzed by immunoblotting. The signal intensity of ABCB1 was plotted as a function of the logarithmic value of membrane protein. Signal intensity = 19.8 log [membrane protein] + 1.59 (R^2 = 0.983). (C) Effect of vanadate on the basal and drug-stimulated ATPase activities. Sf9 plasma membranes (2 μg of protein) expressing ABCB1 WT and variants (A893P, A893S, and A893T) were incubated with ATP (2 mM) and verapamil (20 μM) in the presence of sodium o-vanadate (vanadate) at different concentrations (0, 10, 20, 50, and 100 μM) at 37 °C for 30 min. After the incubation, the amount of liberated phosphate was measured as described in Experimental Procedures. Data are expressed as mean values ± SD (n = 3). (D) Correlation between the drug-stimulated ATPase activity and the amount of ABCB1 protein in Sf9 plasma membrane preparations. The relative amounts of ABCB1 protein in membrane preparations were measured by immunoblotting and quantified, as described above. Sf9 plasma membrane preparations (a total of 2 μg of membrane protein) expressing ABCB1 WT and variants (A893P, A893S, and A893T) were incubated with ATP (2 mM) and verapamil (20 μM) at 37 °C for 30 min. The verapamil-stimulated ATPase activity was determined.

heated from 0 to 310 K (−273 to 37 °C) in 400 ps and equilibrated at 310 K (37 °C) for 100 ps. The time step of the simulations was 2 fs. Temperature was controlled at 310 K (37 °C) by Berendsen's algorithm (*44*). The SHAKE method was applied to constrain all bonds connecting hydrogen atoms (*45*). To represent the effect of membrane environments, harmonic constraints with a strength of 4 kcal/(mol·Å^2) were applied to all atoms in the transmembrane (TM) regions of TM10 (amino acids 858–882) and TM11 (amino acids 945–964). MD calculation was performed to simulate the movement of the intracellular loop located between TM10 and TM11 for each variant protein (A893S, A893T, or A893P) as well as the WT.

Statistical Analysis. Experimental data were expressed as relative values ± SD of more than three experiments. All statistical analyses were performed by using Microsoft Excel 2003 software (Microsoft Co., Redmond, WA). The statistical significance of differences between WT and each variant type was determined according to the two-sided Student's t-test. p values <0.05 or <0.01 were considered statistically significant.

RESULTS

Expression of SNP Variants of ABCB1 in Insect Cells. On the basis of the ABCB1 (WT) cDNA cloned from a human liver cDNA library, those variant forms (i.e., S400N, R492C, R669C, I849M, A893P, A893S, A893T, M986V, A999T, P1051A, and G1063A) were generated by site-directed mutagenesis as described in Experimental Procedures. The variant forms as well as the WT of ABCB1 were then expressed in Sf9 cells by using the pFastBac1 vector and recombinant baculoviruses. The plasma membrane fraction was prepared from those cells. The upper panel of Figure 2A demonstrates the protein levels of those variants and the WT of ABCB1 detected by immunoblotting, where differences in ABCB1 protein levels among the plasma membrane preparations were observed in the signal intensity of immunoblotting. To quantitatively analyze the activity of ABCB1 variants, it is critically important to normalize the expression level of each variant protein. The C219 monoclonal antibody reportedly recognizes the epitopes corresponding to amino acids 568–581 (VVQEALDKARKGRT) and 1213–1226 (VVQEALDKAREGRT) of ABCB1 (*46*), and all of the variants expressed in Sf9 cells had the same epitope

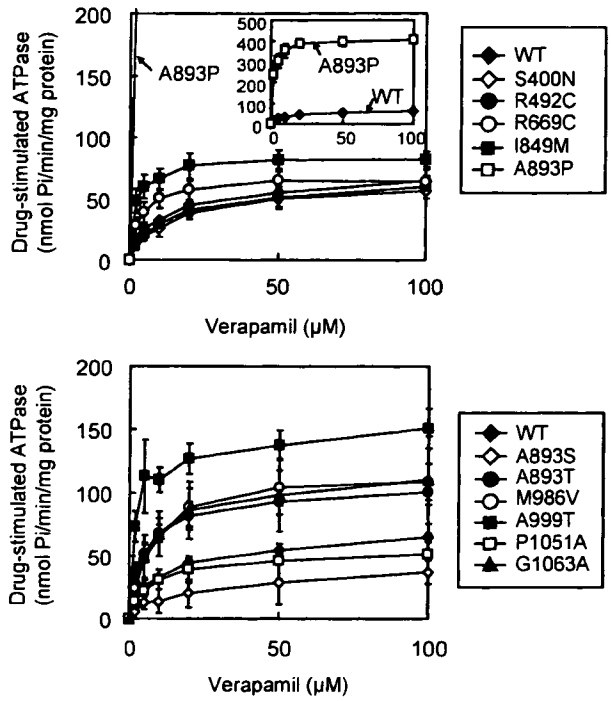

FIGURE 3: Verapamil-stimulated ATPase activity of ABCB1 WT and SNP variants. Sf9 plasma membranes (2 μg of protein) expressing ABCB1 WT and variants (S400N, R492C, R669C, I849M, A893P, A893S, A893T, M986V, A999T, P1051A, and G1063A) were incubated with ATP (2 mM) and verapamil at different concentrations (0, 1, 2, 5, 10, 20, 50, and 100 μM) at 37 °C for 30 min. After the incubation, the amount of liberated phosphate was measured as described in Experimental Procedures. All activities are expressed as mean values ± SD (n = 6).

Table 2: K_m and V_{max} Values for ATPase Activity of ABCB1 WT and Variants toward Verapamil[a]

SNP	K_m (μM)	V_{max} [nmol min^{-1} (mg of protein)$^{-1}$]	V_{max}/K_m
WT	5.8 ± 2.3	62.4 ± 7.8	10.8
S400N	5.8 ± 2.8	46.7 ± 5.3**	8.0
R492C	5.6 ± 1.9	49.6 ± 10.0*	8.9
R669C	3.2 ± 1.6*	64.7 ± 6.9	20.1
I849M	1.5 ± 0.7**	80.3 ± 9.5**	51.8
A893P	1.5 ± 0.5**	405.2 ± 16.5**	274.6
A893S	11.1 ± 5.4	43.1 ± 7.1**	3.9
A893T	4.3 ± 1.4	98.9 ± 9.5**	22.9
M986V	5.1 ± 1.1	114.9 ± 13.6**	22.5
A999T	2.0 ± 0.8**	143.1 ± 21.2**	70.9
P1051A	6.2 ± 3.0	52.1 ± 13.6	8.4
G1063A	6.2 ± 3.7	117.9 ± 16.4**	19.0

[a] Data are expressed as mean ± SD, n = 6. *p < 0.05; **p < 0.01.

sequences. Figure 2B clearly demonstrates a linear relationship between the signal intensity of immunoblotting and the logarithmic value of the amount of protein applied to the electrophoresis. Similar relationships were observed with variants proteins, as well. On the basis of the linear relationship, the expression levels of ABCB1 WT and its variants in different plasma membrane preparations were quantitatively estimated and normalized (Figure 2A, bottom panel).

Effect of Verapamil and Nicardipine on ATPase Activity of ABCB1 WT and Variants. Since verapamil is reportedly a typical substrate for ABCB1, we first tested verapamil-stimulated ATPase activity in the plasma membranes prepared from Sf9 cells expressing ABCB1 WT. Such verapamil-stimulated activity was not detected in the plasma membranes prepared from the control cells infected with mock virus (refer to Figure 10 in ref *32*). Membrane preparations from both control and ABCB1-expressing Sf9 cells exhibited basal ATPase activities that were little affected by o-vanadate at concentrations up to 100 μM (Figure 2C) but inhibited by 1 mM beryllium chloride, a nonspecific ATPase inhibitor (data not shown). On the other hand, the verapamil-stimulated ATPase activity was vanadate-sensitive. As shown in Figure 2C, the drug-stimulated ATPase activities of ABCB1 WT and the A893S, A893T, and A893P variants were completely inhibited by 20 μM o-vanadate. Furthermore, linear correlations were observed between the verapamil-stimulated vanadate-sensitive ATPase activity and the amounts of the ABCB1 protein in Sf9 plasma membranes expressing WT or SNP variants (Figure 2D). Therefore, it is concluded that the drug-stimulated ATPase activity reflects the function of ABCB1 and that the activity could be normalized by considering the ABCB1 protein levels determined by immunoblotting. In this context, we measured the drug-stimulated ATPase activity throughout this study.

Table 3: K_m and V_{max} Values for ATPase Activity of ABCB1 WT and Variants toward Nicardipine[a]

SNP	K_m (μM)	V_{max} [nmol min^{-1} (mg of protein)$^{-1}$]	V_{max}/K_m
WT	1.1 ± 0.6	45.2 ± 8.7	41.0
S400N	1.7 ± 0.8	39.1 ± 9.1	23.4
R492C	1.1 ± 0.5	46.6 ± 6.4	43.5
R669C	0.3 ± 0.3**	53.5 ± 13.1	164.6
I849M	0.8 ± 0.9	80.2 ± 9.6**	102.9
A893P	0.1 ± 0.0**	341.2 ± 36.6**	4858.4
A893S	2.0 ± 0.6	39.2 ± 6.0	19.5
A893T	0.4 ± 0.2**	77.0 ± 16.9**	207.8
M986V	0.7 ± 0.4	89.7 ± 17.7**	129.9
A999T	0.3 ± 0.3**	115.4 ± 21.2**	393.6
P1051A	0.9 ± 0.3	33.1 ± 8.8*	36.3
G1063A	0.8 ± 0.4	93.2 ± 27.6**	121.4

[a] Data are expressed as mean ± SD, n = 6. *p < 0.05; **p < 0.01.

To characterize the effect of nonsynonymous polymorphisms on the ABCB1 function, we measured the verapamil-stimulated ATPase activity by incubating the membrane preparation with verapamil at different concentrations (0–100 μM) for each variant and the WT. Figure 3 depicts the verapamil-stimulated ATPase activity of ABCB1 WT, S400N, R492C, R669C, I849M, A893P, A893S, A893T, M986V, A999T, P1051A, and G1063A, where the verapamil-stimulated ATPase activities are normalized by considering the ABCB1 protein amounts.

As demonstrated in Figure 3, the verapamil-stimulated ATPase activity varied among those variants. For all of the variants tested, saturation kinetics was observed in the relationship between the verapamil-stimulated ATPase activity and the verapamil concentration, suggesting Michaelis–Menten kinetics. Thus, K_m and V_{max} values were calculated from Lineweaver–Burk plots of (verapamil-stimulated ATPase activity)$^{-1}$ vs (verapamil concentration)$^{-1}$ for each variant and WT (data not shown). A893P, I849M, A893T, M986V, and G1063A variants showed higher V_{max} values than did the WT, whereas the V_{max} value of A893S was lower than that of WT. It is noteworthy that the A893P variant

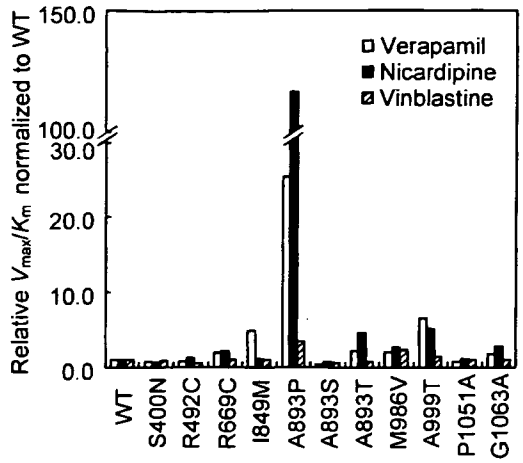

FIGURE 4: V_{max}/K_m values of ABCB1 WT and variants observed for verapamil, nicardipine, and vinblastine. Drug-stimulated ATPase activity of the ABCB1 WT and SNP variants was measured as described in Experimental Procedures. Sf9 plasma membranes (2 μg of protein) expressing ABCB1 were incubated with 2 mM ATP and a drug at different concentrations at 37 °C for 30 min. After the incubation, the amount of liberated phosphate was measured. On the basis of Lineweaver–Burk plots, V_{max} and K_m values were determined, and the relative V_{max}/K_m values of SNP variants were calculated by normalizing to the WT. (The relative V_{max}/K_m value of WT = 1.)

exhibited a markedly high ATPase activity toward verapamil (Figure 3, upper panel). Similar saturation kinetics was also observed with nicardipine, another vasodilator. Tables 2 and 3 summarize the kinetic parameter K_m and V_{max} values for those variants toward verapamil and nicardipine, respectively. Accordingly, the value of V_{max}/K_m has been calculated for each variant.

Figure 4 graphically demonstrates the relative V_{max}/K_m values of SNP variants toward verapamil, nicardipine, and vinblastine. In this graph, the relative V_{max}/K_m values of SNP variants were normalized to those of WT. Among those SNP variants, the A893P variant exhibited a very high value (118-fold) of the relative V_{max}/K_m toward nicardipine (Figure 4). On the other hand, the V_{max}/K_m value of the A893P variant toward vinblastine was only 3-fold higher than that of WT (Figure 4). In contrast, the A893S variant exhibited the lowest value of V_{max}/K_m toward those substrates (Figure 4). These results suggest that nonsynonymous SNPs affect the substrate specificity of ABCB1 as referred to the drug-stimulated ATPase activity.

Profiling of Drug-Stimulated ATPase of ABCB1 WT, A893P, A893S, and A893T. To gain more insight into the effect of nonsynonymous polymorphisms on the substrate specificity of ABCB1, we first tested the substrate specificity of ABCB1 WT and SNP variants by measuring their drug-stimulated ATPase activity toward a total of 41 structurally unrelated test compounds. In this measurement, the concentration of those test compounds was equally 10 μM in the reaction mixture, since this concentration was optimal to obtain the drug-stimulated ATPase activity profile of ABCB1 toward a variety of test compounds. At higher concentrations, certain hydrophobic compounds were not completely dissolved. The test compounds are classified into seven groups, i.e., A, neurotransmitters; B, vasodilators, C, steroids; D, potassium channel modulators; D, nonsteroidal antiinflammatory drugs (NSAIDs); F, anticancer drugs; and G, miscellaneous. Figure 5 demonstrates typical results on the drug-stimulated ATPase activity profiles of ABCB1 WT and A893S, A893T, and A893P variants. Among the 41 different therapeutic drugs and compounds tested here, significantly high drug-stimulated ATPase activities were observed in vasodilators, such as verapamil, diltiazem, bepridil, fendiline, prenylamine, and nicardipine, for ABCB1 WT, A893P, A893S, and A893T. In particular, A893P and A893T variants exhibited higher drug-stimulated ATPase activities toward those vasodilators than did ABCB1 WT. Moderate drug-stimulated ATPase activities were observed toward several anticancer drugs, such as vinblastine, etoposide, actinomycin D, and paclitaxel. In those anticancer drugs also, A893P exhibited the highest value of drug-stimulated ATPase activity among ABCB1 WT and SNP variants.

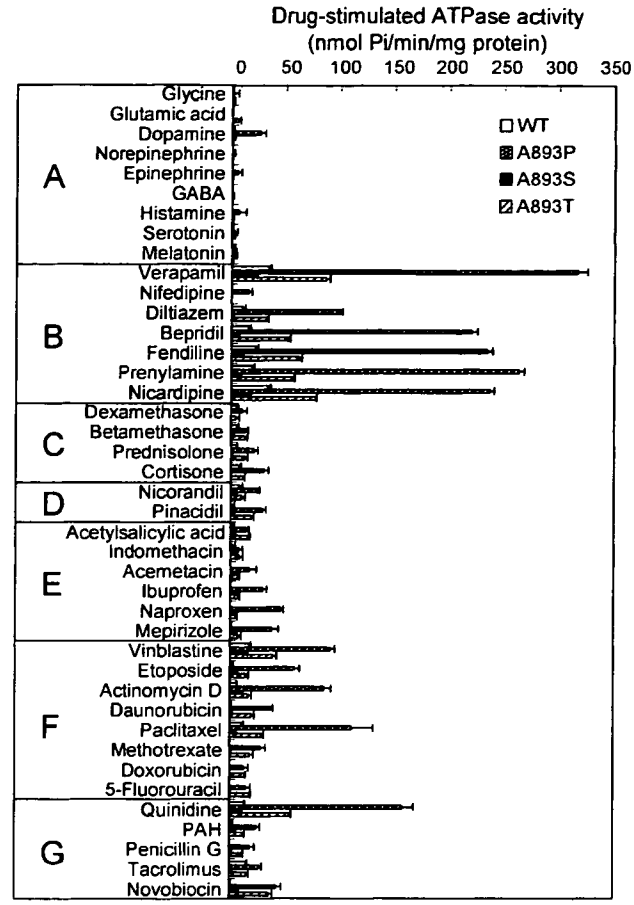

FIGURE 5: Effect of test compounds on the ATPase activity of ABCB1 WT, A893P, A893S, and A893T. The ATPase activity was measured in the presence of 10 μM test compound as described in Experimental Procedures. All activities are expressed as mean values ± SD (n = 4). (A) neurotransmitters; (B) vasodilators, (C) steroids; (D) potassium channel modulators; (E) nonsteroidal antiinflammatory drugs (NSAIDs); (F) anticancer drugs; (G) miscellaneous.

Profiling of Drug-Stimulated ATPase and QSAR Analysis To Evaluate the Substrate Specificity of SNP Variants. The same profiling of drug-stimulated ATPase activities was performed for the other SNP variants to compare with those of ABCB1 WT as well as A893P, A893S, and A893T variants (data not shown). As described above, we have measured the drug-stimulated ATPase activity of all of the prepared SNP variants as well as the WT toward a total of 41 test compounds (10 μM for each in the reaction mixture)

Table 4: Descriptors and Chemical Fragmentation Codes (CFC) Closely Correlated with the ATPase Activity of ABCB1 WT and Variant Proteins[a]

descriptor	CFC	score	description
M532	M532	1.0	two carbocyclic systems with at least one aromatic ring
M132	M132	1.0	ring-linking groups containing 1C atom
C-CHN-BT			one or more carbon chains bonded to ring C, V, C=V, C·V, C=U, C·U, or U applicable
	M281	1.0	one
	M282	2.0	two
	M283	3.0	three or more
ESTR			ester (thioester) group bonded to heterocyclic C via >C=O (>C=S)
	J211	1.0	one
	J212	2.0	two or more
OH-Ar			−OH group bonded to aromatic C
	H441	1.0	one
	H442	2.0	two
	H443	3.0	three
	H444	4.0	four or more
R-CC			carbocyclic systems with at least one aromatic ring
	M531	1.0	one
	M532	2.0	two
	M533	3.0	three or more
RT			ring tertiary N (amine and non-amine)
	H201	1.0	one amine
	H202	2.0	two amines
	H203	3.0	three or more amines
	H211	1.0	one non-amine
	H212	2.0	two non-amines
	H213	3.0	three or more non-amines
-O-Ar			ether with −O− bonded to aromatic C
	H541	1.0	one
	H542	2.0	two
	H543	3.0	three or more
D012	D012	1.0	one atom of fused heterocyclic ring bears substituent(s); atom is not at or adjacent (atom is beta) to ring fusion
G010	G010	1.0	one substituted C atom in an unfused aromatic ring
H100	H100	1.0	one primary amine
H181	H181	1.0	one amine bonded to aliphatic C
H421	H421	1.0	one −OH group bonded to heterocyclic C
H521	H521	1.0	one ether with −O− bonded to heterocyclic C
M113	M113	1.0	benzene linked to other ring (non-benzene or non-aryl ring) by a single or double bond
M232	M232	1.0	carbon chain containing secondary branching
M280	M280	1.0	no 0-valent or monovalent carbon chains present
M313	M313	1.0	3C atoms in polyvalent chain
M332	M332	1.0	straight carbon chain with none of the groups $-CH_3$, $-C{=}CH_2$, or −C·CH
M370	M370	1.0	carbon chain bonded to a ring C and (U and/or C=U and/or C·U) but not to V, C=V, or C·V
M372	M372	1.0	bonded to ring −C and C=U and/or C·U only
M392	M392	1.0	multipliers for codes M350 to M383 (polyvalent carbon chain attachments) twice
M531	M531	1.0	one carbocyclic system with at least one aromatic ring
M540	M540	1.0	no alicyclic systems
H7	H7	1.0	absence of olefinic/acetylinic groups
H8	H8	1.0	absence of ether or hydroxy
L1	L1	1.0	absence of −C≡N, −N≡C
L9	L9	1.0	absence of functional groups in rings

[a] U represents atoms such as O, S, Se, Te, or N. V represents atoms other than C, H, O, S, Se, Te, or N.

by using our high-speed screening system (*32*). On the basis of the drug-stimulated ATPase profiling data, we performed QSAR analysis to elucidate the substrate specificity of the ABCB1 WT and SNP variants. We used the CFCs to describe the chemical structures of a variety of substrates and nonsubstrates for ABCB1. The Markush TOPFRAG was used to generate CFCs for each compound tested. Table 4 provides explanations for descriptors and CFCs generated in the analysis, where some descriptors (e.g., C-CHN-BT, ESTR, OH-Ar, RT, and -O-Ar) represent multiple CFCs. In this way, however, steroids (group C) and actinomycin D (group F) were excluded from this analysis, because the Markush TOPFRAG program does not have an algorithm to generate CFCs for those compounds.

The multiple linear regression analysis was then carried out to obtain a relationship between the drug-stimulated ATPase activity and the CFCs thus generated. Thereby, we could identify one set of descriptors and/or CFCs related to the substrate specificity of each of the ABCB1 WT and SNP variants. The best-fitting models were created by multiple linear regression analysis, where the predicted activity of the drug-stimulated ATPase of ABCB1 was described as a linear combination of CFCs weighted by the corresponding coefficient, $C(i)$ (see Experimental Procedures). Figure 6 demonstrates the relationships between the drug-stimulated ATPase activities observed with 10 μM test compounds and the predicted ATPase activities for ABCB1 WT, A893P, A893S, and A893T. As clearly shown in this figure, the prediction of drug-stimulated ATPase activity was well correlated with the observed values.

We carried out the same QSAR analysis for all of the variants tested in this study, and Table 5 summarizes the

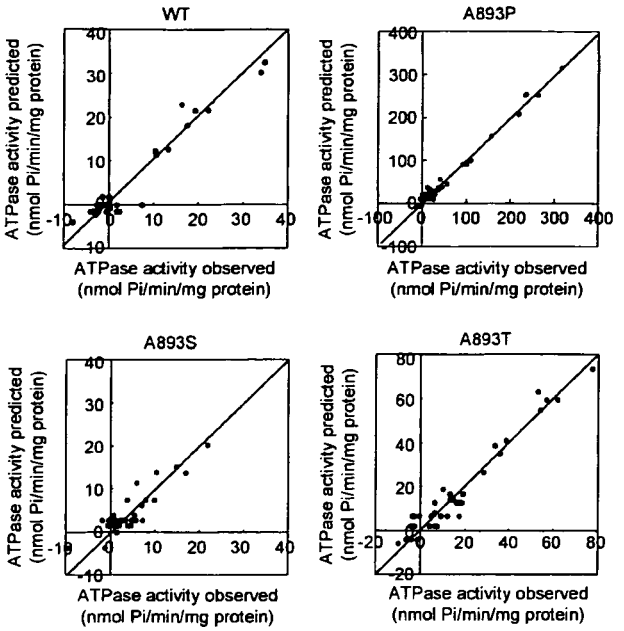

FIGURE 6: Relationships between observed and predicted ATPase activities for ABCB1 WT, A893P, A893S, and A893T. The actual ATP activities were observed with 10 μM test compounds as shown in Figure 5. The predicted ATPase activities were calculated by multiple linear regression analysis performed for ABCB1 WT, A893P, A893S, and A893T.

contents of these multiple linear regression analysis models. The QSAR analysis revealed that the structural components represented by the CFCs of M532 and M132 as well as the descriptor C-CHN-BT commonly contributed to the drug-stimulated ATPase activity of ABCB1 WT and SNP variants. These data suggest that two carbocyclic systems with at least one aromatic ring (M532) as well as ring-linking groups containing one carbon atom (M132) are important structural components for the recognition by ABCB1 WT and SNP variants (Table 5). The values of coefficients corresponding to M532, M132, and C-CHN-BT are plotted for each variant in Figure 7. The values were not equal to ABCB1 WT and those SNP variants. Indeed, the A893P variant exhibited the highest values for the coefficients of M532, M132, and C-CHN-BT. Figure 8 depicts the chemical structures of verapamil, prenylamine, and nicardipine to exemplify the structural components represented by M532, M132, C-CHN-BT, and other descriptors.

In addition to M532, M132, and C-CHN-BT, other structural components also contributed the drug-stimulated ATPase activity of ABCB1 WT and SNP variants, but in unequal manners. As demonstrated in Table 5, the coefficients of CFCs and descriptors varied among WT and those variants. For example, the presence of one substituted carbon atom in an unfused aromatic ring (CFC = G010) negatively contributed the drug-stimulated ATPase activity of the I849M variants, whereas this structural component did not affect the other variants or WT. On the other hand, the benzene structure linked to the other ring by a single or double bond (CFC = M113) negatively contributed to the drug-stimulated ATPase activity of M986V, G1063A, A999T, S400N, and A893S variants and WT, whereas the activity of the other variants was not affected by this structural component. Thus, the variation of coefficients for the CFCs and descriptors listed in Table 5 appears to reflect changes in the substrate specificity owing to alterations of amino acids of ABCB1.

To facilitate our understanding in greater detail, we classified all of the tested compounds according to the CFCs and descriptors (see Table 6). For example, structural components represented by M532 are involved in verapamil, bepridil, and nicardipine, whereas those represented by M132 are in fendiline, prenylamine, and quinidine. Structural components corresponding to the descriptor of C-CHN-BT are widely found in different compounds. By referring to the descriptor coefficients (Table 5) and the corresponding descriptors involved in test compounds (Table 6), we could elucidate differences in the substrate specificity among ABCB1 WT and SNP variants.

MD Simulation. The three-dimensional structure of ABCB1 was generated by homology modeling based on the Sav1866 structure template (*37*). In the resulting homology model of ABCB1, amino acid 893 is located in the intracellular loop region connecting two transmembrane domains, i.e., TM10 and TM11 (Figure 9A). It was assumed that amino acid alterations at this position may change the loop structure and thereby affect the drug-stimulated ATPase activity (see Figures 3 and 4). To examine our hypothesis, we constructed a truncated model that consists of the intracellular loop connected with TM10 and TM11. The initial three-dimensional structure of each truncated model (A893S, A893T, or A893P) was deduced from the homology model of ABCB1. Figure 9B demonstrates the loop structures of WT, A893S, A893T, or A893P calculated from the trajectory data of MD simulations at 310 K (37 °C) for 3 ns. Our molecular dynamic simulation clearly shows that multiple kinks are formed in the intracellular loop between TM10 and TM11 in the A893P protein. The RMSF value of the α carbon of each amino acid residue was calculated from the trajectory data for the intracellular loop of WT, A893S, A893T, and A893P. The A893P variant exhibited notably great fluctuations in the intracellular loop, in particular, at the region of amino acids 910−920 (data not shown).

DISCUSSION

SNPs and Haplotypes in ABCB1. The first investigation into the effects of genetic polymorphisms of ABCB1 on pharmacotherapy was reported in 2000 (*6*). One silent SNP 3435C > T in exon 26 of the *ABCB1* gene was reportedly correlated with ABCB1 expression levels. Since that report was published, a large number of genetic variations of the human *ABCB1* gene have been discovered (*24*, *25*). Table 7 summarizes the allele frequencies of the genetic variants that were investigated in this study.

Recent findings suggest that genetic variation of 3435C > T may not be the single causal modulator of the observed functional differences (*25*). In fact, Horinouchi et al. and Kroetz et al. have provided evidence that the ABCB1 3435 site is in tight linkage disequilibrium with a number of other variant sites, including the 2677G > T variant leading to the Ala893Ser change (A893S) (*8*, *16*). Similar linkage disequilibrium was observed in West Black African populations (*23*). It is likely that genetic variations at position 2677 that result in alterations of amino acid 893 are more directly contributed to interindividual variability in ABCB1 function.

Table 5: ABCB1 WT and Variant-Specific Descriptors and Corresponding Coefficients Deduced from QSAR Analysis[a]

	coefficients (95% reliability) for ABCB1 WT and vatiants											
descriptor	WT	S400N	R492C	R669C	I849M	A893P	A893S	A893T	M986V	A999T	P1051A	G1063A
M532	24.3 (3.76)	21.2 (5.81)	18.5 (5.87)	35.9 (7.68)	52.7 (11.30)	169.8 (18.84)	14.0 (4.03)	61.2 (7.75)	39.4 (8.76)	63.0 (9.39)	13.9 (4.78)	52.1 (10.94)
M132	21.5 (3.89)	14.1 (5.34)	13.6 (5.78)	32.8 (6.89)	61.4 (12.66)	135.6 (22.95)	11.2 (4.06)	52.8 (7.16)	38.2 (8.62)	65.9 (8.44)	7.6 (5.71)	24.3 (10.46)
C-CHN-BT	3.3 (0.72)	3.8 (0.95)	1.7 (0.87)	3.5 (1.08)	5.7 (1.55)	11.6 (2.48)	1.2 (0.65)	6.1 (1.29)	7.1 (1.43)	7.3 (1.44)	2.0 (0.66)	2.8 (1.86)
ESTR				−10.1 (4.93)				−12.5 (5.00)				
OH-Ar									−6.4 (4.03)			
R-CC						16.1 (7.86)					−4.4 (1.73)	
RT		−8.9 (4.21)										−17.7 (8.22)
-O-Ar										5.7 (3.67)		
D012							5.5 (4.10)					
G010					−15.4 (9.59)							
H100			4.9 (3.59)									
H181										−7.3 (5.04)		
H421								14.6 (6.84)				
H521									14.1 (10.42)			
M113	−5.8 (3.69)	−11.7 (5.30)					−7.7 (3.70)		−22.8 (8.75)	−16.4 (8.19)		−16.5 (10.58)
M232												−14.5 (9.38)
M280	4.8 (2.65)											
M313							−5.2 (3.18)					
M332		−5.0 (3.11)										
M370			4.2 (3.14)									
M372				10.0 (5.46)	14.4 (7.91)							
M392						73.3 (25.03)					10.3 (6.38)	
M531			−5.1 (3.05)									
M540						15.8 (11.27)						
H7	7.3 (4.01)				24.0 (10.91)							
H8								10.7 (4.74)				
L1											−6.7 (2.52)	
L9				13.8 (6.93)								
constant	−12.2	−5.5	−0.2	−2.3	−24.0	−7.1	1.3	−4.3	0.9	9.0	0.6	−11.2
R^2	0.934	0.847	0.853	0.906	0.893	0.981	0.782	0.954	0.915	0.956	0.836	0.831
FO(6, 29)	68.9	26.8	28.1	46.4	40.5	254.5	17.3	100.3	51.8	106.2	24.6	23.7
Q^2	0.883	0.710	0.767	0.729	0.826	0.968	0.572	0.923	0.828	0.909	0.617	0.760

[a] R^2, correlation coefficient; FO, Fisher value (level of statistical significance).

Amino Acid 893 Is a "Hot Spot" in the Ethnic-Specific Polymorphisms of ABCB1. The present study addresses the impact of nonsynonymous polymorphisms of ABCB1 (i.e., S400N, R492C, R669C, I849M, A893S, A893T, A893P, M986V, A999T, P1051A, and G1063A) on its function. To evaluate functional changes associated with nonsynonymous polymorphisms in the present study, we measured the ATPase activity of ABCB1 variants by using structurally unrelated test compounds as potential substrates. The measurement of drug-stimulated ATPase activity was widely used by different research groups to investigate the function of ABCB1 (*1*, *33*). We here demonstrate that amino acid 893 is a hot spot in the genetic polymorphisms of ABCB1 in terms of both pharmacological and anthropological aspects.

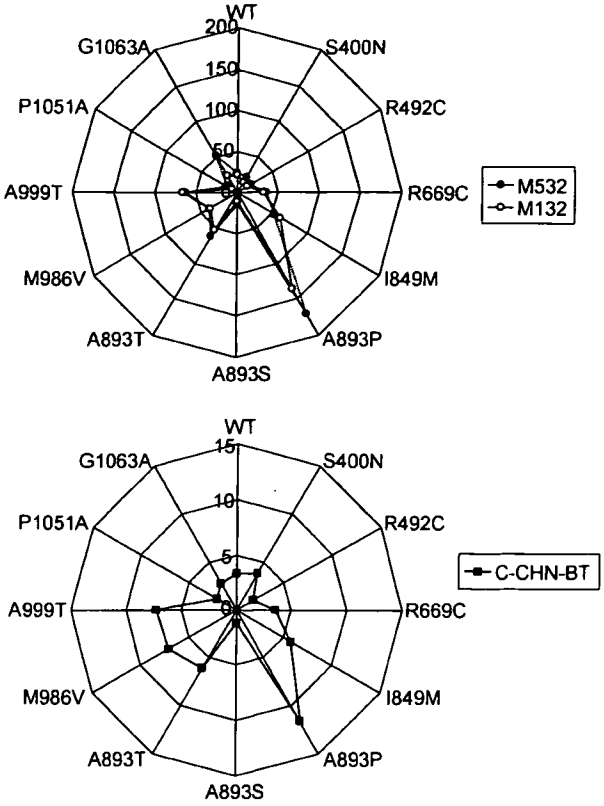

FIGURE 7: Comparison of coefficients for M532 and M132 (upper panel) as well as for C-CHN-BT (lower panel) among ABCB1 WT and SNP variants. The values of those coefficients for WT and SNP variants (i.e., S400N, R492C, R669C, I849M, A893P, A893S, A893T, M986V, A999T, P1051A, and G1063A) are the same as those shown in Table 5.

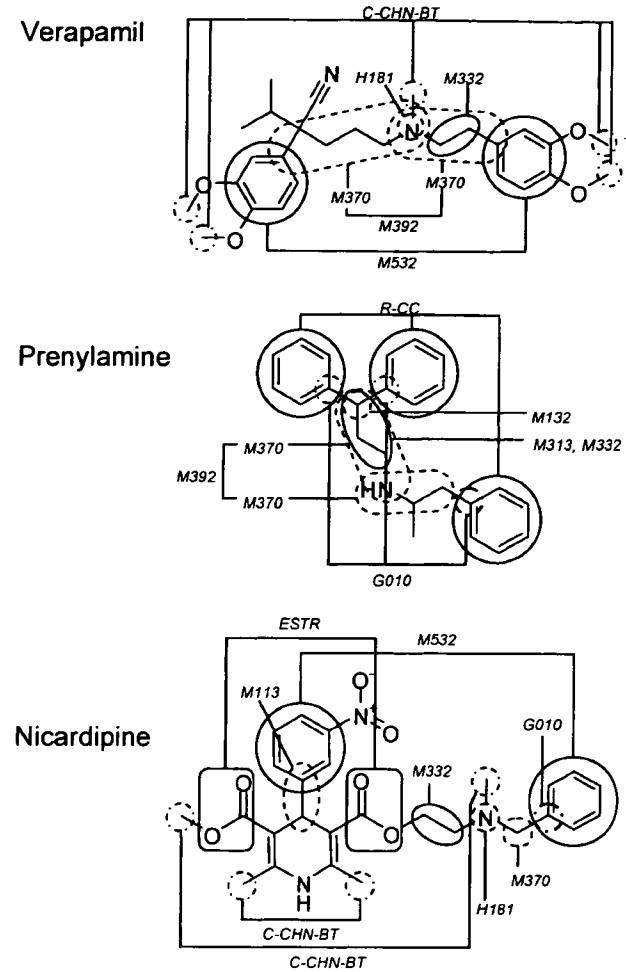

FIGURE 8: Chemical structures of verapamil, prenylamine, and nicardipine and their structural components represented by M532, M132, C-CHN-BT, and other descriptors.

As Horinouchi et al., Kroetz et al., and Allabi et al. reported, the ABCB1 G2677T/A contains a triallelic polymorphism (with G at nucleotide 2677 found in exon 21 of the WT sequence and with A and T at that position comprising the three possible variants), which results in an amino acid change Ala893Ser/Thr (A893S/T) (*8*, *16*, *23*). The polymorphisms of 2677G, 2677T, and 2677A exhibit wide ethnic differences in the allele frequency. It is important to note that the frequency of allele 2677G (Ala893) was the highest in the African population, and it decreases along the order of African-American, Mexican-American, Caucasian, Japanese, Asian-American, and Pacific Islander (Figure 10), suggesting a west−east downward geographical gradient. On the other hand, the frequency of allele 2677A shows a west−east upward geographical gradient (Figure 10). Interestingly, similar west−east upward geographical gradients are observed in the frequencies of the 421A allele of ABCG2 (*47*) and the 538A allele of ABCC11 (*48*). In the case of the genetic polymorphisms of ABCC11, we recently reported that the SNP of 538G > A is responsible for determination of earwax type (*48*). Individuals with dry earwax are AA homozygotes and are frequently observed in Northern China, Japan, and Southern Asia.

In addition to the triallelic polymorphism of 2677G > T/A, the recent NCBI SNP database contains the 2677G > C polymorphism (dbSNP: rs2032582) that results in the A893P variant. This polymorphism has not yet been well validated, and it is regarded as a rare mutation. As shown in Figures 3 and 4 as well as in Tables 2 and 3, the A893P variant exhibited remarkably high ATPase activity toward verapamil and nicardipine in the present study. There is a possibility that increased ATPase activity of this variant protein could be due to a computational method used for normalization of protein levels. However, this explanation may be oversimplified. In fact, the V_{max}/K_m value of the A893P for nicardipine was 2 orders of magnitude (118-fold) greater than that of the WT (Figure 4 and Table 2), whereas the V_{max}/K_m value for vinblastine was only 3-fold greater than that of the WT (Figure 4). These results suggest that the functional impact of the A893P substitution varies depending on the drugs tested. High ATPase activity of this variant was observed toward structurally diverse test compounds as well (Figure 5). It is interesting, but puzzling, that the 2677C allele occurs at an extremely low incidence as compared with the 2677A and 2677T alleles. ABCB1 is located in the apical domain of the enterocytes of the gastrointestinal tract (jejunum and duodenum) and limits the uptake and absorption of xenobiotics from the intestine into the systemic circulation by excreting substrates into the gastrointestinal tract. Therefore, one could assume that, because of the extremely high transport activity of this A893P variant, the uptake of nutrients can also be limited in individuals carrying the 2677C allele. If this assumption were true, it would be likely that those ancient individuals were subjected to stringent natural selection such that the allele frequency might have

Table 6: Classification of Test Compounds According to Descriptors and CFCs

descriptor	CFC	compounds									
M532	M532	verapamil	bepridil	nicardipine							
M132	M132	fendiline	prenylamine	quinidine							
C-CHN-BT	M281	epinephrine	melatonin	verapamil	diltiazem	bepridil	nicardipine	pinacidil	indomethacin	acemetacin	acetylsalicyclic acid
		ibuprofen	naproxen	vinblastine	etoposide	daunorubicin	methotrexate	doxorubicin	quinidine	novobiocin	
	M282	nifedipine	diltiazem	nicardipine	mepirizol	vinblastine	etoposide	paclitaxel	penicillin G	novobiocin	
	M283	verapamil	diltiazem	vinblastine	paclitaxel	tacrolimus					
ESTR	J211	vinblastine									
	J212	nifedipine	nicardipine								
OH-Ar	H441	serotonin	etoposide	novobiocin							
	H442	dopamine	norepinephrine	epinephrine	daunorubicin	doxorubicin					
R-CC	M531	dopamine	norepinephrine	epinephrine	nifedipine	diltiazem	pinacidil	indomethacin	acemetacin	ibuprofen	acetylsalicyclic acid
		naproxen	etoposide	daunorubicin	methotrexate	doxorubicin	PAH	penicillin G	novobiocin		
	M532	verapamil	bepridil	nicardipine							
	M533	fendiline	prenylamine	paclitaxel							
RT	H211	diltiazem	indomethacin	acemetacin	mepirizol						
-O-Ar	H541	melatonin	diltiazem	indomethacin	acemetacin	naproxen	vinblastine	daumorubicin	doxorubicin	quinidine	
D012	D012	vinblastine	etoposide	methotrexate							
G010	G010	bepridil	fendiline	prenylamine	nicardipine	paclitaxel	penicillin G				
H100	H100	glycine	glutamic acid	dopamine	norepinephrine	GABA	histamine	serotonin	daunorubicin	doxorubicin	PAH
H181	H181	glycine	glutamic acid	dopamine	norepinephrine	epinephrine	GABA	histamine	serotonin	verapamil	diltiazem
		bepridil	fendiline	prenylamine	nicardipine	vinblastine					
H421	H421	vinblastine	daunorubicin	doxorubicin	novobiocin						
H521	H521	etoposide	daunorubicin	doxorubicin							
M113	M113	nifedipine	diltiazem	nicardipine							
M232	M232	bepridil	pinacidil	ibuprofen	novobiocin						
M280	M280	glycine	glutamic acid	dopamine	norepinephrine	GABA	histamine	serotonin	fendiline	prenylamine	nicorandil
		5-fluorouracil	PAH								
M313	M313	glutamic acid	bepridil	fendiline	prenylamine	methotrexate	tacrolimus				
M332	M332	glutamic acid	dopamine	norepinephrine	epinephrine	GABA	histamine	serotonin	melatonin	verapamil	diltiazem
		bepridil	fendiline	prenylamine	nicardipine	nicorandil	paclitaxel	methotrexate			
M370	M370	dopamine	norepinephrine	epinephrine	histamine	serotonin	melatonin	verapamil	bepridil	fendiline	prenylamine
		nicardipine	indomethacin	acemetacin	ibuprofen	naproxen	paclitaxel	methotrexate	quinidine	penicillin G	
M372	M372	indomethacin	acemetacin	ibuprofen	naproxen	penicillin G					
M392	M392	verapamil	fendiline	prenylamine							
M531	M531	(refer to above)									
M540	M540	histamine	serotonin	melatonin	nicorandil	naproxen	mepirizol	vinblastine	daunorubicin	doxorubicin	5-fluorouracil
H7	H7	quinidine	glycine	glutamic acid	dopamine	norepinephrine	epinephrine	GABA	histamine	serotonin	melatonin
		verapamil	nifedipine	diltiazem	bepridil	fendiline	prenylamine	nicardipine	nicorandil	pinacidil	acetylsalicylic acid
		indomethacin	acemetacin	ibuprofen	naproxen	mepirizol	vinblastine	etoposide	daunorubicin	paclitaxel	methotrexate
		doxorubicin	5-fluorouracil	PAH	penicillin G						
H8	H8	glycine	glutamic acid	GABA	histamine	nifedipine	fendiline	prenylamine	nicardipine	nicorandil	acetylsalicylic acid
		pinacidil	ibuprofen	methotrexate	5-fluorouracil	PAH	penicillin G				
L1	L1	nifedipine	diltiazem	nicardipine	nicorandil	mepirizol	daunorubicin	methotrexate	doxorubicin	5-fluorouracil	penicillin G
		tacrolimus	novobiocin								
L9	L9	verapamil	nifedipine	nicardipine	nicorandil	pinacidil					

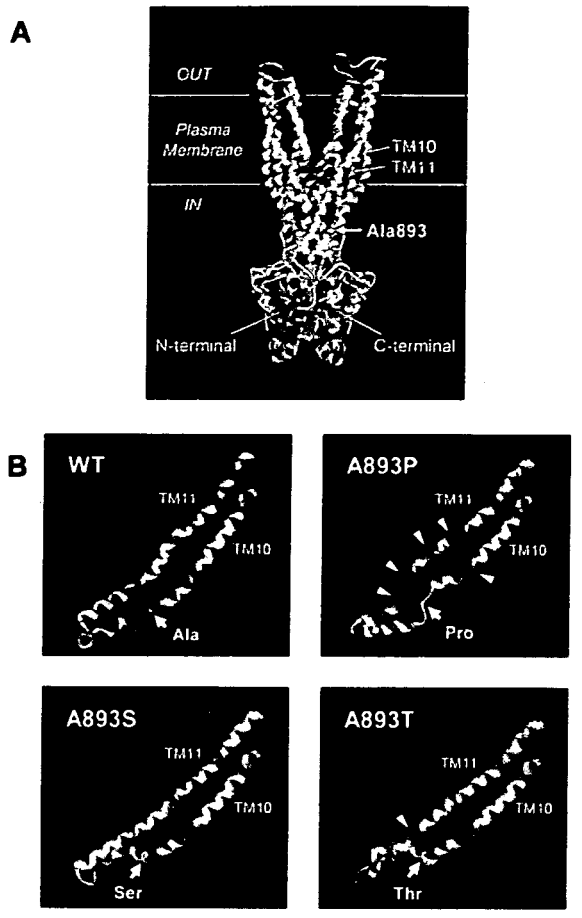

FIGURE 9: (A) Homology model structure of human ABCB1. Homology modeling was performed by using the Sav1866 structure (*37*) as a template. (B) Structure of the intracellular loop between TM10 and TM11 calculated by MD simulation. Detailed conditions used for homology modeling and MD simulation are described in Experimental Procedures.

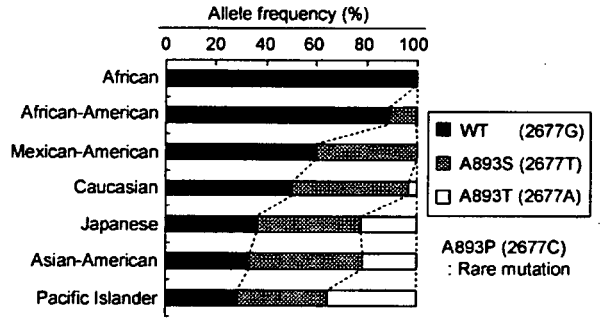

FIGURE 10: Allele frequencies of WT (Ala893), A893S (Ser893), and A893T (Thr893) among different ethnic populations. Those allele frequencies were calculated from the currently available data (*8*, *16*, *23*, *29*–*31*) and are represented as bars in this graph. The A893P (Pro893) variant is a rare mutation (rs2032582) recorded in the NCBI dbSNP database.

been maintained at minimal levels throughout the history of *Homo sapiens*.

In contrast to the A893P variant, the A893S variant exhibited the lowest V_{max}/K_m values toward verapamil or nicardipine among the variants tested (Tables 2 and 3). The 2677T polymorphism causing this A893S variant has recently been reported to be crucial in conferring susceptibility to lung cancer (*49*). It is suggested that the 2677T mutation results in a decreased transport of environmental carcinogens out of pulmonary cells. The A893T variant, on the other hand, exhibited V_{max}/K_m values even higher than those of WT (Tables 2 and 3). Amino acid 893 is located in the intracellular loop between TM10 and TM11 (Figure 1), and amino acid alterations at this position appear to affect the function of ABCB1.

MD Simulation of the Intracellular Loop between TM10 and TM11. Most recently, Dawson and Locher demonstrated the three-dimensional structure of Sav1866, a bacterial ABC transporter (*37*). As with ABCB1, the ATPase activity of Sav1866 was stimulated by doxorubicin and vinblastine (*37*). Sav1866 is a half ABC transporter, showing significant similarity to human ABCB1. In the present study, the putative three-dimensional structure of ABCB1 WT (Figure 9A) was deduced from X-ray crystallography of Sav1866 by means of homology modeling. To understand the molecular mechanisms underlying the observed differences in the ATPase activity among ABCB1 WT, A893P, A893S, and A893T (Figures 3–5), we performed MD simulation based on the homology model of ABCB1.

According to multiple alignments, A893 residing in the second half of human ABCB1 corresponds to V199 of Sav1866. It is important to note that V199 in the Sav1866 structure is located in the cytoplasmic helical stretch in continuity with TM4 before "coupling helix 2". Dawson and Locher emphasize the importance of the intracellular loop regions, in particular, of "coupling helices 1 and 2". In the case of ABCB1, coupling helix 2 corresponds to amino acid residues 903–912. Our MD simulation data (Figure 9B) suggest that the A893P mutation promotes multiple kinks in this cytoplasmic helical region and modifies the interaction of coupling helix 2 with the ATP-binding domain. This may provide an explanation, in part, for the effect of the A893P mutation on ATP hydrolysis. Loo et al. have recently suggested that rearrangement of TM11 may contribute to the release of drug substrate during ATP hydrolysis (*50*). More detailed MD simulation of ABCB1 is presently ongoing in our laboratory, and results will be reported elsewhere.

Functional Evaluation of Genetic Polymorphisms of ABCB1 by QSAR Analysis. Other nonsynonymous polymorphisms, such as S400N, R492C, R669C, P1051A, and G1063A occurring in intracellular loops as well as I849M, M986V, and A999T alterations in transmembrane domains, exhibited moderate changes in the kinetic properties of ABCB1. To understand the impact of those nonsynonymous polymorphisms on the function of ABCB1, it is critically important to quantitatively analyze the functional differences among such variants. To accomplish this, we have developed a method of QSAR analysis. Using the high-speed screening system, we first measure ABCB1 ATPase activity toward a total of 41 different therapeutic drugs and compounds.

On the basis of the ATPase activity data, we could analyze the QSAR to identify multiple sets of CFCs closely linked with the substrate specificity of ABCB1 WT and SNP variants. We used CFCs to describe the chemical structures of a variety of substrates and nonsubstrates for ABCB1. The CFCs were originally created to answer the need for accessing information in the increasing numbers of chemical patents. Derwent Information, Ltd., developed this structure-indexing language, which is suitable for describing chemical